An interferon-driven oxysterol-based defense against tumor-derived extracellular vesicles

[1, 12]Angelica Ortiz, [1, 12]Jun Gui, [1]Farima Zahedi, [1]Pengfei Yu, [1]Christina Cho, [1]Sabyasachi Bhattacharya, [1]Christopher J. Carbone, [1]Qiujing Yu, [1]Kanstantsin V. Katlinski, [1]Yuliya V. Katlinskaya, [1]Simran Handa, [1]Victor Haas, [2]Susan W. Volk, [3]Angela K. Brice, [4]Kim Wals, [4]Nicholas J. Matheson, [4]Robin Antrobus, [5, 6]Sonja Ludwig, [5]Theresa L. Whiteside, [7]Cindy Sander, [7]Ahmad A. Tarhini, [7]John M. Kirkwood, [4]Paul J. Lehner, [8]Wei Guo, [9]Hallgeir Rui, [10]Andy J. Minn, [10]Constantinos Koumenis, [11]J. Alan Diehl, and [1, 13, *]Serge Y. Fuchs

[1]Department of Biomedical Sciences, School of Veterinary Medicine, University of Pennsylvania, Philadelphia, PA 19104, USA
[2]Department of Department of Clinical Sciences & Advanced Medicine, School of Veterinary Medicine, University of Pennsylvania, Philadelphia, PA 19104, USA
[3]Department of Pathobiology, School of Veterinary Medicine, University of Pennsylvania, Philadelphia, PA 19104, USA
[4]Department of Medicine, Cambridge Institute for Medical Research, Cambridge Biomedical Campus, Cambridge, CB2 0XY, UK
[5]Departments of Pathology, Immunology and Otolaryngology, University of Pittsburgh School of Medicine, Pittsburgh, PA 15213, USA
[6]Department of Otorhinolaryngology, University of Duisburg-Essen, Germany
[7]Department of Medicine, University of Pittsburgh School of Medicine, Pittsburgh, PA 15213, USA
[8]Department of Biology, University of Pennsylvania, Philadelphia, PA 19104, USA
[9]Department of Pathology, Medical College of Wisconsin, Milwaukee, WI 53226; USA
[10]Department of Radiation Oncology, Perelman School of Medicine, University of Pennsylvania, Philadelphia, PA 19104, USA.
[11]Department of Biochemistry, Hollings Cancer Center, Medical University of South Carolina, Charleston, SC 29425, USA
[12]These authors contributed equally
[13] Lead Contact

* Correspondence: syfuchs@upenn.edu, tel. 1-(215)-573-6949

Key words: metastasis, adjuvant therapy, extracellular vesicles, melanoma, 25-hydroxycholesterol, reserpine, interferon

SUMMARY

Tumor-derived extracellular vesicles (TEV) “educate” healthy cells to promote metastases. We found that melanoma TEV downregulated type I interferon (IFN) receptor and expression of IFN-inducible cholesterol 25-hydroxylase (*CH25H*). CH25H produces 25-hydroxycholesterol, which inhibited TEV uptake. Low *CH25H* levels in leukocytes from melanoma patients correlated with poor prognosis. Mice incapable of downregulating the IFN receptor and *Ch25h* were resistant to TEV uptake, TEV-induced pre-metastatic niche and melanoma lung metastases; however, ablation of *Ch25h* reversed these phenotypes. An antihypertensive drug reserpine suppressed TEV uptake and disrupted TEV-induced formation of the pre-metastatic niche and melanoma lung metastases. These results suggest the importance of CH25H in defense against education of normal cells by TEV and argue for use of reserpine in adjuvant melanoma therapy.

SIGNIFICANCE

Education of normal cells by factors delivered via the tumor-derived vesicles promotes tumor growth, progression and metastasis. Results of this study uncover the key role of CH25H in defense against normal cells education by tumor-derived vesicles and, accordingly, against melanoma progression and metastatic disease. In addition, these data provide a proof-of-principle for interfering with tumor-derived extracellular vesicles uptake as a strategy for adjuvant treatment of metastatic melanoma and suggest the repurpose of reserpine for such application.

INTRODUCTION

Whereas metastases are the most important determinants of cancer lethality (Chaffer and Weinberg, 2011), there is a relative dearth of clinically validated specific targets and agents that either eliminate the existing metastatic lesions, or, at the very least prevent initial metastases and suppress their colonization (Steeg, 2016). Normal cells in target organs can form a hospitable "soil" (Fuchs, 1882; Paget, 1889) enabling malignant cells to home and colonize. Given genomic instability and extreme plasticity of malignant cells, targeting these normal cells might represent a promising therapeutic strategy against metastatic disease.

The metastatic process in many cancer types is stimulated by tumor-derived extracellular vesicles (TEV), including exosomes (Costa-Silva et al., 2015; Peinado et al., 2012). These vesicles can dramatically affect normal cells by delivering biomolecules that alter the function of these cells (Aleckovic and Kang, 2015; Becker et al., 2016; Kalluri, 2016; Lobb et al., 2017; Peinado et al., 2012). Such "education" by TEV can co-opt normal cells to contribute to tumor progression and metastasis via multiple mechanisms including formation of the pre-metastatic niches in distant healthy organs such as the lungs (Liu et al., 2016; Lobb et al., 2017).

However, the majority of normal cells in a tumor-bearing organism exhibits limited uptake of TEV (Mendt et al., 2018) and appears to remain unaffected suggesting the existence of yet to be identified defensive mechanisms that restrict the extent of education by TEV. Here we sought to identify the nature of such defenses in normal cells as well as potential mechanisms underlying their breach and failure during tumor progression and metastasis. In addition, we aimed to identify and characterize the agents that can disrupt the education of normal cells by TEV and thus may have therapeutic activities in the adjuvant/neoadjuvant setting.

RESULTS

TEV inactivate the IFN pathway to facilitate TEV uptake and education of normal cells

TEV-driven education of normal cells is attributed to transfer of diverse biomolecules including signaling receptors (reviewed in (Aleckovic and Kang, 2015; Becker et al., 2016; Kalluri, 2016; Lobb et al., 2017; Peinado et al., 2012)). We used a Stable Isotope Labeling by Amino Acids in Cell Culture (SILAC)-based Plasma Membrane Profiling proteomic screen (Matheson et al., 2015; Weekes et al., 2013) (Figure S1a) to determine changes in the repertoire of cell surface signaling receptors in human cells exposed to TEV (characterized in Figure S1b). Comparative mass spectrometry revealed that TEV treatment decreased the levels of several plasma membrane proteins (Table S1) including the IFNAR1 chain of the type I interferon (IFN) receptor (Figure 1a). We further focused on IFNAR1 because of the important role of IFN in defense against tumor metastases (Parker et al., 2016) and clinical use of these cytokines in adjuvant therapy of melanoma (Eggermont et al., 2014).

TEV derived from melanoma cells did not alter the levels of *IFNAR1* mRNA (Figure S1c) but notably decreased IFNAR1 protein (Figure 1b and S1d) without inducing activation of STAT1 (Figure S1d) suggesting that TEV downregulate IFNAR1 in an IFN-independent manner. Previous reports demonstrated that non-ligand stimuli activate p38α protein kinase-dependent phosphorylation of IFNAR1 on Ser residues (Bhattacharya et al., 2011). This phosphorylation enables the βTrcp E3 ubiquitin ligase to facilitate IFNAR1 ubiquitination and degradation (Bhattacharya et al., 2013; Fuchs, 2013; Huangfu et al., 2012; Liu et al., 2009; Qian et al., 2011). Given that TEV encompass diverse types of RNA that can trigger a number of signaling cascades including p38 activation (Liu et al., 2016), we examined the impact of TEV on this pathway. TEV treatment had a modest effect on βTrcp but activated p38 kinase (Figure S1d) and stimulated IFNAR1 Ser phosphorylation and ubiquitination (Figure 1c). Furthermore, a p38 inhibitor prevented IFNAR1 loss (Figure S1e) suggesting that TEV act as inducers of p38-dependent IFNAR1 downregulation.

To determine the relevance of these observations to naturally occurring melanoma, we examined whether extracellular vesicles isolated from melanoma patients can downregulate IFNAR1 and whether

IFNAR1 is indeed downregulated in normal cells from melanoma patients. Plasma-derived vesicles from melanoma patients (but not from healthy donors) indeed decreased the levels of IFNAR1 protein but not mRNA in human cells in vitro (Figure 1d and S1f). Furthermore, lower levels of the cell surface IFNAR1 protein (but not mRNA) were found in leukocytes from melanoma patients compared to those from healthy donors (Figure 1e and S1g). Importantly, the extent of IFNAR1 downregulation was greater in patients with documented metastatic lesions (Figure 1e). Given that an increase in TEV was associated with metastatic melanoma (Peinado et al., 2012), these data are consistent with downregulation of IFNAR1 on normal cells as a hallmark of their education by TEV in patients.

Understanding of importance of IFNAR1 downregulation as a part of education of normal cells by TEV requires modeling the effects of TEV in vitro and in vivo. Extracellular vesicles isolated from cultured B16F10 mouse melanoma cells (but not from normal primary mouse lung fibroblasts) robustly induced p38 kinase activation and downregulated IFNAR1 in primary mouse splenocytes (Figure 1f). Furthermore, ablation of *Mapk14* (gene that encodes p38α) in these splenocytes attenuated the loss of IFNAR1 upon exposure to TEV (Figure 1g) suggesting that normal mouse cells can recapitulate the p38-driven loss of IFNAR1.

In order to evaluate the importance of TEV-induced downregulation of IFNAR1, we used *Ifnar1*^{S526A} knock-in mice, which are deficient in IFNAR1 ubiquitination and degradation (characterized in (Bhattacharya et al., 2014; Katlinski et al., 2017) and henceforth termed “SA”). SA splenocytes were resistant to TEV-induced downregulation of IFNAR1 in vitro (Figure 1g). Furthermore, intravenous injection of TEV in vivo downregulated IFNAR1 levels on the surface of wild-type (WT) (but not SA) leukocytes (Figure S1h). Finally, lower levels of IFNAR1 on peripheral blood leukocytes were detected in tumor-bearing WT (but not SA) mice compared to naive animals (Figure 1h) indicating that SA cells and animals can be used as controls for assessing the importance of IFNAR1 loss in TEV-induced education.

IFNAR1 is required for all effects of Type I IFN but not Type II IFNγ (Platanias, 2005). Accordingly, pre-treatment of mouse cells with TEV attenuated phosphorylation of STAT1 induced specifically by IFNβ but not by IFNγ (Figure 2a and S2a) suggesting that TEV can inactivate IFNAR1 signaling. Whereas extracellular vesicles from normal fibroblasts induced expression of some of IFN-stimulated genes (ISG) consistent with a previous report (Boelens et al., 2014), TEV notably suppressed this expression (Figure 2b). An even greater suppression of ISG was elicited by multiple treatments imitating continuous education by TEV (Figure S2b). These observations in mouse cells were faithfully recapitulated in human cells where expression of ISG was inhibited by extracellular vesicles from melanoma patients (but not from healthy donors, Figure 2c) indicating that TEV can inactivate the IFN-IFNAR1 pathway.

The ISG were not suppressed if cells were exposed to IFN before TEV (Figure S2c) indicating that IFN may cancel the effect of TEV. Importantly, control experiments revealed that pre-treatment of cells with IFN impeded TEV uptake in splenocytes (Figure 2d and S2d). These results may suggest that IFN and TEV can mutually counteract each other's effects: whereas IFNAR1 will be inactivated in cells first exposed to TEV, signaling through active IFNAR1 should limit the education by TEV.

Indeed, SA cells resistant to TEV-induced IFNAR1 downregulation (Figure 1g-h, S1h) also did not respond to TEV by decreasing IFN signaling (Figure 2a and S2a) or the ISG expression (Figure 2b). Importantly, SA cells were relatively refractory to TEV uptake in vitro compared to WT or *Ifnar1*-null cells (Figures 2d, e and S2d, e). TEV uptake in SA cells was restored by neutralizing antibody against IFNAR1 (Figures 2e and S2e) demonstrating a critical role of IFNAR1 signaling in this phenotype. The SA mice were also resistant to in vivo uptake of TEV by splenocytes and bone marrow cells (Figure 2f and S2f). These results suggest the importance of IFNAR1 in limiting TEV uptake and TEV-elicited education of normal cells.

TEV administration in vivo was shown to educate normal cells and induce the pre-metastatic niche in the lungs characterized by pulmonary myeloid infiltration and fibronectin deposition (Kaplan et al.,

2005; Peinado et al., 2012). Intriguingly, treatment of WT (but not SA) mice with TEV led to a notable loss of IFNAR1 protein (Figure 3a) and decreased ISG mRNAs (Figure 3b) in lung tissues. These results suggest that education of normal cells by TEV in vivo includes inactivation of IFNAR1 signaling and further justifies using SA animals as a negative control in experiments assessing the importance of this education.

Consistent with published results (Peinado et al., 2012) we found that administration of TEV promoted formation of the $CD11b^+$ myeloid clusters (Figure 3c and S3a), and fibronectin deposits (Figure 3d and S3b) in the lungs of WT mice. Importantly, lung tissues from TEV-treated SA mice exhibited fewer $CD11b^+$ cell clusters or fibronectin deposits and lower overall lung myeloid infiltration compared to WT mice (Figures 3c-d and S3b-c). Given that poor myeloid infiltration in SA lungs was reversed by administration of the neutralizing antibody against IFNAR1 (Figure S3d), these data suggest that formation of the TEV-induced pre-metastatic niche requires inactivation of IFNAR1 and ensuing disruption of the IFNAR1-mediated defenses against education of normal cells by TEV.

Lyden and co-authors demonstrated a notable stimulation of primary tumor growth and metastases in irradiated host mice that received transfer of the educated bone marrow from TEV-treated donor mice (Peinado et al., 2012) (Figure 3e). Consistent with this report, we found that transplantation of bone marrow from TEV-treated WT mice indeed stimulated lung metastases in WT recipients inoculated with B16F10 tumors (Figures 3f). Importantly, we did not observe such stimulation when bone marrow was taken from TEV-treated SA mice (Figure 3f). These results suggest that IFNAR1 in normal cells is important to interrupt their education by TEV and, consequently, to provide defense against TEV-stimulated metastases.

IFN-induced CH25H limits uptake of TEV and interrupts the education of normal cells

We next sought to determine how IFNAR1 signaling can suppress TEV uptake and disrupt TEV-induced education of normal cells. Uptake of extracellular vesicles can occur through a number of

mechanisms including phagocytosis, endocytosis, micropinocytosis, direct membrane fusion, etc (French et al., 2017). Bone marrow macrophages from SA mice were not deficient in phagocytosis compared to WT macrophages (Figure S4a). Fortuitously, we also observed that IFN suppressed the uptake of empty protein-less liposomes (Figure S4b) suggesting an inhibitory effect of IFN on lipid membrane fusion, which is involved in many types of TEV uptake (French et al., 2017).

Indeed effects of IFN on lipid membrane fluidity have been previously reported (Chatterjee et al., 1982). Recent findings suggest that cholesterol 25-hydroxylase (CH25H), an enzyme generating 25-hydroxycholesterol (25HC) that alters membrane characteristics (Luu and Moog, 1991) can be induced by IFN (Anggakusuma et al., 2015; Blanc et al., 2013; Liu et al., 2013). Pre-treatment of cells with 25HC suppressed uptake of liposomes in WT cells as well as in cells lacking *Ifnar1* or *Ch25h* (Figure S4b) suggesting that this oxysterol acts downstream of these genes. Cells exposed to 25HC also exhibited a decreased uptake of TEV (Figure 4a and S4c). Importantly, IFN did not inhibit uptake of liposomes or TEV in cells lacking *Ch25h* (Figure 4a and S4b-c). Furthermore, ablation of *Ch25h* in SA mice restored the ability of tissues from these animals to uptake TEV in vivo (Figures 4b and S4d) suggesting that *Ch25h* acts downstream of IFNAR1 to restrict the education of normal cells by TEV.

Of note, TEV downregulated *Ch25h* expression whereas vesicles from primary fibroblasts did not (Figure S4e). Opposite effects on *Ch25h* were elicited by IFN and TEV, but these stimuli did not affect other monooxygenases involved in cholesterol oxidation such as *Cyp46a* and *Cyp27a* (Figure S4e). Tissues from naive SA mice expressed higher levels of *Ch25h* compared to those from WT mice (Figure S4f). Furthermore, WT cells exposed to TEV in vitro exhibited lower levels of *Ch25h* compared to those from SA mice (Figure 4c). Importantly, administration of TEV in vivo decreased *Ch25h* in lung tissues from WT but not SA mice (Figure 4d) indicating the importance of IFNAR1 loss for downregulation of *Ch25h*. Remarkably, ablation of *Ch25h* in SA mice restored TEV-induced formation of pre-metastatic niche as seen from accumulation of $CD11b^{+}$ clusters and fibronectin deposits in the lungs (Figure 4e).

This result indicates a defensive role of the IFNAR1-CH25H pathway against TEV-induced education of normal cells and the ensuing development of a pre-metastatic niche.

Suboptimal bioavailability of 25HC (Li et al., 2017) prompted us to search for small molecules that can mimic the suppressive effects of this oxysterol on TEV uptake. A limited hypothesis-driven screen tested the agents previously reported to inhibit biological processes that involve lipid membrane fusion such as viral membrane fusion (Boriskin et al., 2006; Shoemaker et al., 2013) , neuromediator re-uptake (Erickson et al., 1992), maturation of myocytes and osteoclasts (Bar-Sagi and Prives, 1983; Okazaki et al., 1999; Yamashita et al., 2010), etc (Table S2). Among six tested compounds, the anti-hypertensive drug reserpine was found to interfere with B16F10 TEV uptake by mouse splenocytes or bone marrow cells (Figure S5a). These results were further validated in vitro in human cells (Figure 5a and S5b).

Furthermore, administration of reserpine in vivo also suppressed TEV uptake (Figure 5b and S5c), prevented TEV-induced downregulation of IFNAR1 (Figure 5c) and stimulated ISG including *Ch25h* (Figure S5d) in normal cells. Importantly, treatment with reserpine abolished TEV-induced formation of the pre-metastatic niche as evident from analysis of lung myeloid infiltrates and fibronectin deposits (Figure 5d and S5e). These results suggest that reserpine can be used to disrupt TEV-induced education of normal cells and the generation of the pre-metastatic niche.

Anti-metastatic role of the IFNAR1-CH25H pathway and potential for adjuvant therapy utilizing inhibitors of TEV uptake

Given that the IFNAR1-dependent expression of *Ch25h* limits the education of normal cells by TEV, which, in turn, can stimulate tumor metastases (Chin and Wang, 2016a; Chin and Wang, 2016b; Costa-Silva et al., 2015; Peinado et al., 2012; Peinado et al., 2011), we sought to examine the putative anti-metastatic role of this pathway. First, we evaluated its status in human melanoma. Extracellular vesicles isolated from melanoma patients (but not healthy donors) decreased *CH25H* expression in human cells in vitro (Figure 6a). In addition, leukocytes from melanoma patients with metastatic disease expressed

less *CH25H* than healthy donors or melanoma patients without metastases (Figure 6b). Furthermore, melanoma patients expressing lower *CH25H* than the average level in healthy donors had increased occurrence of distant metastases (Figure 6c) and displayed a poor survival (Figure 6d). These results suggest that downregulation of *CH25H* in normal cells may breach the *CH25H*-mediated defenses against melanoma progression and metastases.

To further examine this possibility we used a syngeneic metastatic tumor model in mice harboring WT or SA IFNAR1. In these experiments, we did not administer additional TEV but rather relied on TEV production by subcutaneous B16F10 tumors, which were shown to generate abundant endogenous TEV (Liu et al., 2016; Peinado et al., 2012). Many more of disseminated B16F10-TdTomato cells were found in the lungs of WT mice compared to SA animals (Figure S6a-b) indicating the importance of IFNAR1 inactivation for efficient metastatic process.

A delayed growth of primary B16F10 tumors observed in SA mice (Figure S6c) was similar to other tumor models (Katlinskaya et al., 2016; Katlinski et al., 2017). This delay was partially alleviated by knockout of *Ch25h* in SA mice. Resection of tumors growing in SA mice was postponed until they reached a volume ~200 mm^2 similar to that in other genotypes (Figure S6c). At that point, we excised primary tumors and examined post-surgical survival and appearance of lung metastases. Under these conditions, WT and *Ch25h*$^{-/-}$ mice developed massive lung metastatic disease (Figure 6e-f) that led to 100% lethality within a month (Figure 6g). When primary tumors of similar size were resected from SA mice, they displayed virtually no detectable lung metastases and a dramatic improvement in post-surgical survival (Figure 6e-f-g). These data further support the importance of IFNAR1 signaling in normal cells in protection against metastatic disease.

Remarkably, the ablation of *Ch25h* in SA mice completely reversed the suppression of lung metastases (Figure 6e-f) and abolished the extended survival (Figure 6g). This result suggest that CH25H acts epistatically downstream of IFNAR1 to elicit the defenses against tumor metastasis in normal cells.

Given that the IFNAR1-CH25H pathway also protects these normal cells against TEV uptake (Figure 4b) and pre-metastatic niche-stimulating education by TEV (Figure 4e), it is plausible that preventing education by TEV may restore the defenses against metastases, for example, in the context of adjuvant or neoadjuvant therapies.

Thus, we examined the anti-metastatic activities of reserpine that can inhibit TEV uptake (Figure 5a-b), remediate the loss of IFNAR1 and *Ch25h* (Figures 5c and S5d) and disrupt formation of TEV-induced pre-metastatic niche (Figure 5d). Reserpine treatment of B16F10 cells in vitro did not dramatically affect their proliferation (Figure S7a) or characteristics of produced TEV (Figure S7b) or ability of these TEV to induce the myeloid infiltration in the lungs in vivo (Figure S7c).

We next assessed the effects of reserpine in the B16F10 tumor-bearing mice. Early studies reported that administration of reserpine inhibited tumor growth but attributed this effect to a severely tranquilized state and dramatic loss of weight due to a failure of sleeping animals to eat or drink for protracted periods of time (Belkin and Hardy, 1957; Burton et al., 1957). Here we used moderate reserpine doses, which were well tolerated and did not decrease animal weight throughout the experiments (Figure S7d). Importantly, reserpine treatment restored IFNAR1 levels in peripheral blood leukocytes (Figure 7a) and upregulated *Ch25h* and other ISGs in the lungs of tumor-bearing animals (Figure S7e) suggesting a successful disruption of education of normal cells by endogenously produced TEV.

When administered alone, reserpine had rather modest effects on primary tumor growth (Figure S7f) and cancer-related survival (Figure 7b) indicating its limited utility as a single agent. We next examined the efficacy of reserpine in the context of adjuvant/neo-adjuvant therapy (Figure 7c). Primary tumors were grown to ~200 mm^2 (Figure S7g) followed by their surgical removal and reserpine was administered before and after surgery (Figure 7c). Although recurrence of primary tumors and tumors growing in the lymph nodes (that were not removed during the surgery) forced the euthanasia of some

of animals, the overall survival was significantly improved by reserpine (Figure 7d). Subsequent analysis showed that reserpine virtually eliminated lung metastases (Figure 7e-f) indicating a great potency of reserpine as an adjuvant therapeutic agent.

DISCUSSION

Data presented here suggest that IFNAR1-mediated expression of CH25H in healthy tissues limits the extent of education of these tissues by TEV and, accordingly, restricts the overall area of the pre-metastatic niche in the lungs. Accordingly, these results suggest a defensive role of the IFNAR1-CH25H pathway against development of distant lung metastases. Whereas limited analysis of leukocytes from melanoma patients is suggestive of association between the loss of *CH25H* and poor disease outcome, future extensive studies should determine the value of *CH25H* expression as potential prognostic biomarker in patients with melanoma and other highly metastatic cancers.

Among other signaling pathways, activation of p38 kinase was observed during the education of normal lung cells by TEV that encompass RNA and other damage-associated molecular patterns (Liu et al., 2016). Whereas activation of p38 is important for TEV-driven loss of IFNAR1, additional studies should characterize the nature of these diverse (and likely redundant) TEV-carried substances that elicit IFNAR1 inactivation. Given that *CH25H* is an IFN-inducible gene (Anggakusuma et al., 2015; Liu et al., 2013) and knockout of this gene abolishes the suppression of metastases in mice that maintain the expression of downregulation-resistant IFNAR1 mutant, it is likely that CH25H functions downstream of IFNAR1.

Accordingly, continuous exposure to TEV and TEV-induced loss of IFNAR1 may contribute to suppression of this defensive pathway in normal cells. Despite re-synthesis of IFNAR1, its rapid ubiquitination and degradation in cells, which encounter TEV before IFN, would further stimulate uptake of TEV and, thereby, perpetuate the positive feedback loop of IFNAR1/CH25H inactivation. In turn, this

positive feedback would ensure continuous education of normal cells leading to generation of the metastatic niches and promoting cancer metastasis.

Conversely, enabling normal cells to restore IFNAR1 and respond to IFN by induction of CH25H is expected to interrupt the education by TEV. Indeed, IFN counteracts the effects of TEV on normal cells through maintaining CH25H expression and limiting TEV uptake. It remains to be determined, which of many types of TEV uptake (e.g. endocytosis, macropinocytosis, direct fusion, etc) are regulated by CH25H. Although CH25H product 25HC can act as a ligand for activating the nuclear Liver X Receptor (that can play anti-tumorigenic roles) a number of oxysterol-elicited effects were shown to be independent of the Liver X Receptor (reviewed in (Traversari et al., 2014)). Importantly, another ligand of this receptor, 27-hydroxycholesterol, was recently shown to promote the metastatic process through acting on immune cells (Baek et al., 2017). Notably, IFN did not induce the expression of Cyp27a, which catalyzes production of 27-hydroxycholesterol. Regardless of these considerations and, given that anti-tumorigenic agonists of the Liver X Receptor are being developed (Flaveny et al., 2015), future studies should determine its role in 25HC-dependent protection of normal cells against TEV education.

Furthermore, 25HC and reserpine may possess additional anti-tumorigenic activities unrelated to their ability to restrict TEV uptake. Although we did not observe that reserpine affects TEV production or ability of these TEV to educate normal cells, additional mechanisms of action for reserpine cannot be entirely ruled out. Independent of these considerations, our data suggest that reserpine (and perhaps other agents capable of disrupting TEV-induced education) can elicit potent adjuvant therapeutic activities.

Limited benefits of IFN in patients who already have developed distant metastases restricts application of IFN to the sphere of adjuvant/neoadjuvant therapy (Eggermont et al., 2014; Tarhini et al., 2012) aimed to disrupt the pre-metastatic niche and limit metastatic colonization. Our findings that protection of normal cells can be compromised by TEV-induced IFNAR1/CH25H downregulation argues

for shifting the strategy towards IFNAR1- and CH25H-independent modalities such as a low-dose reserpine regimen. Given that metastasis is a progressive process involving continuous education of normal cells, reserpine might be relevant not only for preventing this process but also for restricting the ongoing metastatic expansion. Being approved by the FDA since 1955 and deemed tolerable for patients with conditions far less grave than metastatic cancer, the clinical efficacy of reserpine in the context of adjuvant melanoma therapy should be tested posthaste.

SUPPLEMENTAL INFORMATION

Supplemental Information includes Supplemental Experimental Procedures, seven figures, and two tables and can be found with this article online.

ACKNOWLEDGEMENTS

This work was supported by the NIH/NCI PO1 CA165997 grant (to C.K., J.A.D., and S.Y.F.), R01 grants CA092900, CA216936 and CA188575 (to S.Y.F. and H.R.), The Wellcome Trust (PRF 101835/Z/13/Z to P.J.L.), MRC (CSF MR/P008801/1 to N.J.M.) and NHSBT (WPA15-02 to N.J.M.)as well as by additional support from F32 CA206431 (to A.O.), T32 CA115299 (to S.B.), T32 CA009140 (to K.V.K.), the Pittsburgh-Essen-Partnership Program (to S.L.), Undergraduate Student Scholars Program in the Center for Molecular Studies in Digestive and Liver Disease, University of Pennsylvania (to S.H.) and the Merial Veterinary Scholars Program Fellowship (to V.H.). We thank Ze'ev Ronai and the members of Gabrilovich, Fuchs, Diehl, Koumenis, and Minn labs for critical suggestions

AUTHOR CONTRIBUTIONS

S.Y.F., A.O., J.G., N.J.M., T.L.W., J.M.K., P.J.L., W.G., H.R., A.J.M., C.K., and J.A.D designed the research; A.O., J.G., F.Z., P.Y., C.C., S.B., C.J.C., Q.Y., K.V.K., Y.V.K., S.H., V.H., S.W.V., A.K.B., K.W., N.J.M., R.A., S.L., C.S., A.A.T., and S.Y.F. performed the experiments and interpreted the data, S.Y.F., A.O., J.G., N.J.M., H.R., C.K. and J.A.D. wrote the manuscript with the help of all authors.

DECLARATION OF INTERESTS: All authors declare no competing financial interests

REFERENCES

Aleckovic, M., and Kang, Y. (2015). Regulation of cancer metastasis by cell-free miRNAs. Biochim Biophys Acta *1855*, 24-42.

Anggakusuma, Romero-Brey, I., Berger, C., Colpitts, C. C., Boldanova, T., Engelmann, M., Todt, D., Perin, P. M., Behrendt, P., Vondran, F. W.*, et al.* (2015). Interferon-inducible cholesterol-25-hydroxylase restricts hepatitis C virus replication through blockage of membranous web formation. Hepatology *62*, 702-714.

Baek, A. E., Yu, Y. A., He, S., Wardell, S. E., Chang, C. Y., Kwon, S., Pillai, R. V., McDowell, H. B., Thompson, J. W., Dubois, L. G.*, et al.* (2017). The cholesterol metabolite 27 hydroxycholesterol facilitates breast cancer metastasis through its actions on immune cells. Nat Commun *8*, 864.

Bar-Sagi, D., and Prives, J. (1983). Trifluoperazine, a calmodulin antagonist, inhibits muscle cell fusion. The Journal of cell biology *97*, 1375-1380.

Becker, A., Thakur, B. K., Weiss, J. M., Kim, H. S., Peinado, H., and Lyden, D. (2016). Extracellular Vesicles in Cancer: Cell-to-Cell Mediators of Metastasis. Cancer Cell *30*, 836-848.

Belkin, M., and Hardy, W. G. (1957). Effect of reserpine and chlorpromazine on sarcoma 37. Science *125*, 233-234.

Bhattacharya, S., HuangFu, W. C., Dong, G., Qian, J., Baker, D. P., Karar, J., Koumenis, C., Diehl, J. A., and Fuchs, S. Y. (2013). Anti-tumorigenic effects of Type 1 interferon are subdued by integrated stress responses. Oncogene *32*, 4214-4221.

Bhattacharya, S., HuangFu, W. C., Liu, J., Veeranki, S., Baker, D. P., Koumenis, C., Diehl, J. A., and Fuchs, S. Y. (2010). Inducible priming phosphorylation promotes ligand-independent degradation of the IFNAR1 chain of type I interferon receptor. The Journal of biological chemistry *285*, 2318-2325.

Bhattacharya, S., Katlinski, K. V., Reichert, M., Takano, S., Brice, A., Zhao, B., Yu, Q., Zheng, H., Carbone, C. J., Katlinskaya, Y. V.*, et al.* (2014). Triggering ubiquitination of IFNAR1 protects tissues from inflammatory injury. EMBO Mol Med *6*, 384-397.

Bhattacharya, S., Qian, J., Tzimas, C., Baker, D. P., Koumenis, C., Diehl, J. A., and Fuchs, S. Y. (2011). Role of p38 protein kinase in the ligand-independent ubiquitination and down-regulation of the IFNAR1 chain of type I interferon receptor. The Journal of biological chemistry *286*, 22069-22076.

Blanc, M., Hsieh, W. Y., Robertson, K. A., Kropp, K. A., Forster, T., Shui, G., Lacaze, P., Watterson, S., Griffiths, S. J., Spann, N. J.*, et al.* (2013). The transcription factor STAT-1 couples macrophage synthesis of 25-hydroxycholesterol to the interferon antiviral response. Immunity *38*, 106-118.

Boelens, M. C., Wu, T. J., Nabet, B. Y., Xu, B., Qiu, Y., Yoon, T., Azzam, D. J., Twyman-Saint Victor, C., Wiemann, B. Z., Ishwaran, H.*, et al.* (2014). Exosome transfer from stromal to breast cancer cells regulates therapy resistance pathways. Cell *159*, 499-513.

Boriskin, Y. S., Pecheur, E. I., and Polyak, S. J. (2006). Arbidol: a broad-spectrum antiviral that inhibits acute and chronic HCV infection. Virology journal *3*, 56.

Burton, R. M., Goldin, A., Humphreys, S. R., and Venditti, J. M. (1957). Antileukemic action of reserpine. Science *125*, 156-157.

Chaffer, C. L., and Weinberg, R. A. (2011). A perspective on cancer cell metastasis. Science *331*, 1559-1564.

Chatterjee, S., Cheung, H. C., and Hunter, E. (1982). Interferon inhibits Sendai virus-induced cell fusion: an effect on cell membrane fluidity. Proc Natl Acad Sci U S A *79*, 835-839.

Chin, A. R., and Wang, S. E. (2016a). Cancer-derived extracellular vesicles: the 'soil conditioner' in breast cancer metastasis? Cancer Metastasis Rev.

Chin, A. R., and Wang, S. E. (2016b). Cancer Tills the Premetastatic Field: Mechanistic Basis and Clinical Implications. Clin Cancer Res *22*, 3725-3733.

Costa-Silva, B., Aiello, N. M., Ocean, A. J., Singh, S., Zhang, H., Thakur, B. K., Becker, A., Hoshino, A., Mark, M. T., Molina, H.*, et al.* (2015). Pancreatic cancer exosomes initiate pre-metastatic niche formation in the liver. Nat Cell Biol *17*, 816-826.
Eggermont, A. M., Spatz, A., and Robert, C. (2014). Cutaneous melanoma. Lancet *383*, 816-827.
Erickson, J. D., Eiden, L. E., and Hoffman, B. J. (1992). Expression cloning of a reserpine-sensitive vesicular monoamine transporter. Proc Natl Acad Sci U S A *89*, 10993-10997.
Flaveny, C. A., Griffett, K., El-Gendy Bel, D., Kazantzis, M., Sengupta, M., Amelio, A. L., Chatterjee, A., Walker, J., Solt, L. A., Kamenecka, T. M., and Burris, T. P. (2015). Broad Anti-tumor Activity of a Small Molecule that Selectively Targets the Warburg Effect and Lipogenesis. Cancer Cell *28*, 42-56.
French, K. C., Antonyak, M. A., and Cerione, R. A. (2017). Extracellular vesicle docking at the cellular port: Extracellular vesicle binding and uptake. Semin Cell Dev Biol *67*, 48-55.
Fuchs, E. (1882). Das Sarkom des Uvealtractus. Graefe's Arch Ophthalmol, Wien *XII*.
Fuchs, S. Y. (2013). Hope and fear for interferon: the receptor-centric outlook on the future of interferon therapy. Journal of interferon & cytokine research : the official journal of the International Society for Interferon and Cytokine Research *33*, 211-225.
Goldman, L. A., Zafari, M., Cutrone, E. C., Dang, A., Brickelmeier, M., Runkel, L., Benjamin, C. D., Ling, L. E., and Langer, J. A. (1999). Characterization of antihuman IFNAR-1 monoclonal antibodies: epitope localization and functional analysis. J Interferon Cytokine Res *19*, 15-26.
Huangfu, W. C., Qian, J., Liu, C., Liu, J., Lokshin, A. E., Baker, D. P., Rui, H., and Fuchs, S. Y. (2012). Inflammatory signaling compromises cell responses to interferon alpha. Oncogene *31*, 161-172.
Kalluri, R. (2016). The biology and function of exosomes in cancer. J Clin Invest *126*, 1208-1215.
Kaplan, R. N., Riba, R. D., Zacharoulis, S., Bramley, A. H., Vincent, L., Costa, C., MacDonald, D. D., Jin, D. K., Shido, K., Kerns, S. A.*, et al.* (2005). VEGFR1-positive haematopoietic bone marrow progenitors initiate the pre-metastatic niche. Nature *438*, 820-827.
Katlinskaya, Y. V., Katlinski, K. V., Yu, Q., Ortiz, A., Beiting, D. P., Brice, A., Davar, D., Sanders, C., Kirkwood, J. M., Rui, H.*, et al.* (2016). Suppression of Type I Interferon Signaling Overcomes Oncogene-Induced Senescence and Mediates Melanoma Development and Progression. Cell Rep *15*, 171-180.
Katlinski, K. V., Gui, J., Katlinskaya, Y. V., Ortiz, A., Chakraborty, R., Bhattacharya, S., Carbone, C. J., Beiting, D. P., Girondo, M. A., Peck, A. R.*, et al.* (2017). Inactivation of Interferon Receptor Promotes the Establishment of Immune Privileged Tumor Microenvironment. Cancer Cell *31*, 194-207.
Li, C., Deng, Y. Q., Wang, S., Ma, F., Aliyari, R., Huang, X. Y., Zhang, N. N., Watanabe, M., Dong, H. L., Liu, P.*, et al.* (2017). 25-Hydroxycholesterol Protects Host against Zika Virus Infection and Its Associated Microcephaly in a Mouse Model. Immunity *46*, 446-456.
Liu, J., Carvalho, L. P., Bhattacharya, S., Carbone, C. J., Kumar, K. G., Leu, N. A., Yau, P. M., Donald, R. G., Weiss, M. J., Baker, D. P.*, et al.* (2009). Mammalian casein kinase 1alpha and its leishmanial ortholog regulate stability of IFNAR1 and type I interferon signaling. Mol Cell Biol *29*, 6401-6412.
Liu, S. Y., Aliyari, R., Chikere, K., Li, G., Marsden, M. D., Smith, J. K., Pernet, O., Guo, H., Nusbaum, R., Zack, J. A.*, et al.* (2013). Interferon-inducible cholesterol-25-hydroxylase broadly inhibits viral entry by production of 25-hydroxycholesterol. Immunity *38*, 92-105.
Liu, Y., Gu, Y., Han, Y., Zhang, Q., Jiang, Z., Zhang, X., Huang, B., Xu, X., Zheng, J., and Cao, X. (2016). Tumor Exosomal RNAs Promote Lung Pre-metastatic Niche Formation by Activating Alveolar Epithelial TLR3 to Recruit Neutrophils. Cancer Cell *30*, 243-256.
Lobb, R. J., Lima, L. G., and Moller, A. (2017). Exosomes: Key mediators of metastasis and pre-metastatic niche formation. Semin Cell Dev Biol *67*, 3-10.
Luu, B., and Moog, C. (1991). Oxysterols: biological activities and physicochemical studies. Biochimie *73*, 1317-1320.

Matheson, N. J., Sumner, J., Wals, K., Rapiteanu, R., Weekes, M. P., Vigan, R., Weinelt, J., Schindler, M., Antrobus, R., Costa, A. S*., et al.* (2015). Cell Surface Proteomic Map of HIV Infection Reveals Antagonism of Amino Acid Metabolism by Vpu and Nef. Cell Host Microbe *18*, 409-423.
Mendt, M., Kamerkar, S., Sugimoto, H., McAndrews, K. M., Wu, C. C., Gagea, M., Yang, S., Blanko, E. V. R., Peng, Q., Ma, X*., et al.* (2018). Generation and testing of clinical-grade exosomes for pancreatic cancer. JCI Insight *3*.
Okazaki, R., Toriumi, M., Fukumoto, S., Miyamoto, M., Fujita, T., Tanaka, K., and Takeuchi, Y. (1999). Thiazolidinediones inhibit osteoclast-like cell formation and bone resorption in vitro. Endocrinology *140*, 5060-5065.
Paget, S. (1889). The distribution of secondary growths in cancer of the breast. Lancet *133*, 571-573.
Parker, B. S., Rautela, J., and Hertzog, P. J. (2016). Antitumour actions of interferons: implications for cancer therapy. Nat Rev Cancer *16*, 131-144.
Peinado, H., Aleckovic, M., Lavotshkin, S., Matei, I., Costa-Silva, B., Moreno-Bueno, G., Hergueta-Redondo, M., Williams, C., Garcia-Santos, G., Ghajar, C*., et al.* (2012). Melanoma exosomes educate bone marrow progenitor cells toward a pro-metastatic phenotype through MET. Nat Med *18*, 883-891.
Peinado, H., Lavotshkin, S., and Lyden, D. (2011). The secreted factors responsible for pre-metastatic niche formation: old sayings and new thoughts. Semin Cancer Biol *21*, 139-146.
Platanias, L. C. (2005). Mechanisms of type-I- and type-II-interferon-mediated signalling. Nat Rev Immunol *5*, 375-386.
Qian, J., Zheng, H., Huangfu, W. C., Liu, J., Carbone, C. J., Leu, N. A., Baker, D. P., and Fuchs, S. Y. (2011). Pathogen recognition receptor signaling accelerates phosphorylation-dependent degradation of IFNAR1. PLoS Pathog *7*, e1002065.
Sharma, P., Ludwig, S., Muller, L., Hong, C. S., Kirkwood, J. M., Ferrone, S., and Whiteside, T. L. (2018). Immunoaffinity-based isolation of melanoma cell-derived exosomes from plasma of patients with melanoma. J Extracell Vesicles *7*, 1435138.
Shoemaker, C. J., Schornberg, K. L., Delos, S. E., Scully, C., Pajouhesh, H., Olinger, G. G., Johansen, L. M., and White, J. M. (2013). Multiple cationic amphiphiles induce a Niemann-Pick C phenotype and inhibit Ebola virus entry and infection. PloS one *8*, e56265.
Steeg, P. S. (2016). Targeting metastasis. Nat Rev Cancer *16*, 201-218.
Tarhini, A. A., Floros, T., Lin, H. M., Lin, Y., Rahman, Z., Ashraf, M., Vallabhaneni, P., Sander, C., Rao, U. N. M., Panelli, M*., et al.* (2017). A unique gene expression signature is significantly differentially expressed in tumor-positive or tumor-negative sentinel lymph nodes in patients with melanoma. Melanoma Res *27*, 429-438.
Tarhini, A. A., Gogas, H., and Kirkwood, J. M. (2012). IFN-alpha in the treatment of melanoma. J Immunol *189*, 3789-3793.
Traversari, C., Sozzani, S., Steffensen, K. R., and Russo, V. (2014). LXR-dependent and -independent effects of oxysterols on immunity and tumor growth. Eur J Immunol *44*, 1896-1903.
Weekes, M. P., Antrobus, R., Talbot, S., Hor, S., Simecek, N., Smith, D. L., Bloor, S., Randow, F., and Lehner, P. J. (2012). Proteomic plasma membrane profiling reveals an essential role for gp96 in the cell surface expression of LDLR family members, including the LDL receptor and LRP6. J Proteome Res *11*, 1475-1484.
Weekes, M. P., Tan, S. Y., Poole, E., Talbot, S., Antrobus, R., Smith, D. L., Montag, C., Gygi, S. P., Sinclair, J. H., and Lehner, P. J. (2013). Latency-associated degradation of the MRP1 drug transporter during latent human cytomegalovirus infection. Science *340*, 199-202.
Weekes, M. P., Tomasec, P., Huttlin, E. L., Fielding, C. A., Nusinow, D., Stanton, R. J., Wang, E. C., Aicheler, R., Murrell, I., Wilkinson, G. W*., et al.* (2014). Quantitative temporal viromics: an approach to investigate host-pathogen interaction. Cell *157*, 1460-1472.

Yamashita, M., Otsuka, F., Mukai, T., Yamanaka, R., Otani, H., Matsumoto, Y., Nakamura, E., Takano, M., Sada, K. E., and Makino, H. (2010). Simvastatin inhibits osteoclast differentiation induced by bone morphogenetic protein-2 and RANKL through regulating MAPK, AKT and Src signaling. Regulatory peptides *162*, 99-108.
Yu, Q., Zhao, B., Gui, J., Katlinski, K. V., Brice, A., Gao, Y., Li, C., Kushner, J. A., Koumenis, C., Diehl, J. A., and Fuchs, S. Y. (2015). Type I interferons mediate pancreatic toxicities of PERK inhibition. Proc Natl Acad Sci U S A *112*, 15420-15425.

Figure Legends

Figure 1: TEV downregulate IFNAR1 in normal cells

A. Volcano plot summarizing SILAC-based plasma membrane profiling results from THP-1 cells treated with 1205Lu human melanoma TEV. Mean log2(fold change) and -log10(p value) are shown for 366 proteins identified by >1 unique peptide and quantitated in every replicate. Downregulated proteins with a fold change >2 and p<0.05 are outlined in red.
B. Representative histogram of IFNAR1 cell surface levels measured by flow cytometry on THP-1 cells treated with 1205Lu human melanoma TEV (10 μg/10^6 cells for 2 hr) or PBS
C. Effects of TEV (10 μg/10^6 cells for 30 min) on IFNAR1 phosphorylation and ubiquitination in THP-1 cells. Immunoblot (IB) analyses of immunoprecipitated (IP) IFNAR1 using indicated antibodies are shown. Immunoblot analysis of βTRCP and GADPH levels in the whole cell lysate are also shown.
D. Flow cytometry analysis of IFNAR1 cell surface levels on THP-1 cells treated with extracellular vesicles (5 μg for 2 hr) isolated from plasma of healthy donors (HDEV, n=8) or melanoma patients (MPEV, n=13) or PBS (n=7). A representative histogram (top) and quantification (bottom) are shown.
E. IFNAR1 cell surface levels on peripheral blood leukocytes from healthy donors (HD; n=10) or melanoma patients (MP) from two independent cohorts: MP1 (40 patients of stages I-IV) and MP2 20 patients in each of two groups that were positive (SLN^+) or negative (SLN^-) for sentinel lymph node metastases. A representative histogram (top) and ΔMFI quantification (bottom) are shown.
F. Effect of extracellular vesicles from B16F10 (TEV, 10 μg/10^6 cells, 2 hr) or from primary mouse lung fibroblasts (FEV, 20 μg/10^6 cells, 2 hr) on IFNAR1 surface level (analyzed by flow cytometry, top) or p38 activation (analyzed by immunoblotting, bottom) in primary mouse splenocytes.
G. Effect of B16F10 TEV treatment (10 μg/10^6 cells for 2 hr) on IFNAR1 surface level on splenocytes of indicated genotypes.
H. Analysis of IFNAR1 cell surface levels on peripheral blood leukocytes from WT and SA mice (naive or bearing B16F10 tumors of equal size ~200 mm^2, each n=4)

Data are represented as mean ± SEM; p values: * p<0.05; ** p<0.01; *** p<0.001; NS, not significant from unpaired Student's t test (panels A, D, E, H).
See also **Figure S1 and Table S1**

Figure 2: TEV and IFN counteract effects of each other

A. Effect of pre-treatment with B16F10 TEV (10 μg/10^6 cells for 90 min) on activation of STAT1 by IFNβ (250 IU/mL for 30 min) or IFNγ (50 IU/mL for 30 min) in indicated mouse splenocytes analyzed by immunoblotting.
B. qPCR analysis of mRNA for indicated genes in indicated mouse splenocytes treated with PBS, or extracellular vesicles from primary lung fibroblasts (FEV, n=3), or B16F10 (TEV, n=8) at 10 μg for 4 hr.
C. qPCR analysis of mRNA for indicated genes in THP-1 cells treated with PBS (n=7) or with vesicles (5 μg for 4 hr) from healthy donors (HDEV) (n=8) or melanoma patients (MPEV). (n=13)
D. Uptake of DiD-labeled B16F10 TEV (10 μg for 4 hr) by WT or SA splenocytes pre-treated with PBS or mouse IFNβ (1000 IU/mL for 8 hr); n=6 for each group.
E. Uptake of DiD-labeled B16F10 TEV (10 μg for 4 hr) by indicated splenocytes (10^6/mL) pre-treated with IgG control or anti-IFNAR1 (0.33 μg/mL for 1 hr); n=6 for each group.
F. In vivo uptake of i.v. administered DiD-labeled B16F10 TEV (30 μg for 24 hr) by splenocytes and bone marrow cells of indicated mice; n=6 for each group.

Data are represented as mean ± SEM; p values: * p<0.05; ** p<0.01; *** p<0.001; NS, not significant from Student's t test.
See also **Figure S2**

Figure 3: Inactivation of IFNAR1 promotes education of normal cells by TEV and generation of the pre-metastatic niche

A. Immunofluorescence and quantification of IFNAR1 levels in lung tissues collected from indicated mice treated with indicated TEV (8 μg, 3x per week, 3 weeks). Red, IFNAR1; Blue, DAPI; Scale bar, 100 μm; Quantification representing averages from 10 random fields in sections from each of 3 different animals is shown in the right panel
B. qPCR analysis of mRNA for indicated genes from lung tissues from panel A
C. Immunofluorescence analysis of $CD11b^+$ (green) clusters (>2 cells) in the lungs of WT and SA animals treated with PBS or B16F10 TEV (i.v., 8 μg 3x per week, 3 weeks). Scale bar - 100 μm; quantification representing averages from 7 random fields in sections from each of 3 different animals is shown in the bottom panel
D. Immunofluorescence analysis of fibronectin (green) deposits in the lungs of WT and SA animals treated with PBS or B16F10 TEV (i.v., 8 μg 3x per week, 3 weeks). Scale bar, 100 μm; quantification representing averages from 7 random fields in sections from each of 3 different animals is shown in the bottom panel.
E. Schematic of the experiments to evaluate the education of WT and SA bone marrow-derived cells by TEV and effect of this education on B16F10 tumor growth and metastasis
F. Analysis and quantification of lungs from the td-Tomato-B16F10 tumors-bearing WT hosts that received GFP^+ bone marrow derived cells (BMDCs) from WT or SA mice educated or not by TEV. Scale bar, 100 μm. Quantification represents averages from 7 random fields in sections from each of four different animals is shown in the right panel.

Data are represented as mean ± SEM; p values: * $p<0.05$; *** $p<0.001$; NS, not significant from Student's t test.
See also **Figure S3**

Figure 4: CH25H functions downstream of IFNAR1 to limit education of normal cells by TEV

A. Uptake of DiD-labeled B16F10 TEV (10 μg for 4 hr) by splenocytes from indicated mice pre-treated with IFNβ (1000 IU/mL for 8 hr) or 25HC (4 μM for 2 hr) or vehicles as indicated; n=6 for each group.
B. Analysis of DiD^+ splenocytes and bone marrow cells isolated from mice of indicated genotypes 24 hr after i.v. administration of DiD-labeled B16F10 (30 μg); n=6 for each group.
C. qPCR analysis of relative *Ch25h* mRNA levels in B16-F10 TEV-treated (10 μg, 4 hr) splenocytes or bone marrow cells of indicated genotypes (value of 1.0 ascribed to untreated WT cells) ; n=4 for each group.
D. qPCR analysis of relative mRNA levels of *Ch25h* and other genes encoding cholesterol monooxygenases (*Cyp27a* and *Cyp46a*) in the lungs of WT or SA mice administered with PBS or B16F10 TEV (i.v., 8 μg, 3x per week, 3 weeks); n=4 for each group.
E. Analysis of $CD11b^+$ cell clusters and fibronectin deposits in the lungs of indicated mice treated with B16-F10 TEV (i.v., 8 μg, 3x per week, 3 weeks). Quantifications averaging from 7 random fields in sections from each of three different animals are shown. Scale bar, 100 μm.

Data are represented as mean ± SEM; p values: * $p<0.05$; ** $p<0.01$; *** $p<0.001$; NS, not significant from Student's t test.
See also **Figure S4**

Figure 5: Reserpine suppresses education of normal cells by TEV

A. Uptake of DiD-labeled 1205Lu TEV (10 μg for 4 hr) by THP-1 cells pre-treated with vehicle or reserpine (10 μM for 2 hr); n=3 for each group.
B. Uptake of DiD-labeled B16F10 TEV (30 μg) by splenocytes and bone marrow cells isolated from WT mice 24 hr after i.p. injection of vehicle or reserpine (1 μg/kg i.p., given 30 min before TEV injection) followed by i.v. administration of TEV; n=6 for each group.
C. Flow cytometry analysis of IFNAR1 levels on $CD45^+$ peripheral blood leukocytes isolated from WT mice administered i.v. treatment with PBS or B16F10 TEV (8 μg, 3x per week, 3 weeks) and receiving i.p. vehicle or reserpine treatment (as in panel B) as indicated; n=3 for each group.
D. Immunofluorescence analysis of $CD11b^+$ cell clusters and fibronectin deposits in the lungs of WT mice receiving i.p. vehicle or reserpine treatment (as in panel B) followed by i.v. treatment with B16F10 TEV (8 μg, 3x per week, 3 weeks).

Data are represented as mean ± SEM; p values: * $p<0.05$; ** $p<0.01$; *** $p<0.001$; NS – not significant from Student's t test.
See also **Figure S5 and Table S2**

Figure 6: The IFNAR1-CH25H pathway protects against melanoma progression and metastasis

A. qPCR analysis of *CH25H* mRNA levels in THP-1 cells treated with extracellular vesicles from healthy donors (HDEV, n=8)or melanoma patients (MPEV, n=13).
B. qPCR analysis of *CH25H* mRNA levels in blood leukocytes from healthy donors (HD, n=10) or melanoma patients with (MET, n=17) or without (Non-MET, n=20) documented metastatic disease.
C. Documented distant metastases in MP whose lymphocytes expressed greater ($CH25H^{high}$) or lower ($CH25H^{low}$) levels of *CH25H* mRNA compared to healthy donors (HD); Fisher's exact test: p value = 0.000661
D. Kaplan-Meier analysis of survival of melanoma patients classified as $CH25H^{high}$ or $CH25H^{low}$
E. Representative H&E staining of lungs from indicated mice harvested 30 days after resection of s.c. B16F10 tumors of ~200 mm^2. Examples of metastatic lesions are pointed by arrowheads.
F. Quantification of total area of metastatic load in lungs from mice of indicated genotypes from panel E
G. Kaplan-Meier analysis of cancer-related survival of indicated mice that underwent resection of B16F10 tumors as described in panel E.

Data are represented as mean ± SEM; p values: * $p<0.05$; ** $p<0.01$; *** $p<0.001$; NS, not significant from Student's t test (panels A, B, F), Fisher test (panel C) or log-rank test (panels D, G).
See also **Figure S6**

Figure 7: Activity of reserpine in the context of adjuvant/neoadjuvant therapy

A. Flow cytometry analysis of IFNAR1 cell surface levels on peripheral blood leukocytes from naive WT mice (n=4) or WT mice bearing similar sized B16F10 tumors treated with vehicle or reserpine (i.p. 1 mg/kg, 3x per week for 1 week; n=6 each).
B. Kaplan-Meier survival analysis of B16F10 tumor bearing mice treated with vehicle or reserpine (i.p. 1 mg/kg every 48 hr for 1 week)
C. Schematic description of experiments assessing activity of reserpine as neoadjuvant/adjuvant therapeutic agent
D. Kaplan-Meier analysis of cancer-related survival of mice described in panel C.
E. Quantification of total area of metastatic load in lungs from mice described in panel C (Vehicle n=12, Reserpine n=16).

F. H&E staining of lungs from mice treated with vehicle or reserpine as in panel C and harvested 30 days after surgery. Examples of metastatic lesions are pointed by arrowheads.

Data are represented as mean ± SEM; p values: * $p<0.05$; ** $p<0.01$; *** $p<0.001$ from Student's t test (panels A, E) or log-rank test (panels B, D).
See also **Figure S7**

STAR METHODS

Contact for Reagent and Resource Sharing

Further information and requests for resources and reagents should be directed to and will be fulfilled by the Lead Contact, Serge Y. Fuchs (syfuchs@vet.upenn.edu)

EXPERIMENTAL MODEL and SUBJECT DETAILS

Animal Studies

All experiments with animals were carried out under the protocol 803995 approved by the Institutional Animal Care and Use Committee (IACUC) of The University of Pennsylvania. All mice were of C57Bl/6 background and had water and chow ad libitum. Mice were maintained in a specific pathogen-free facility in accordance with American Association for Laboratory Animal Science guidelines. Littermate animals from different cages were randomly assigned into the experimental groups. These randomized experimental cohorts were either co-housed or systematically exposed to other groups' bedding to ensure equal exposure to all group's microbiota. *Ch25h*$^{-/-}$ and *Ifnar1*$^{-/-}$ mice were obtained from the Jackson Laboratory. Littermate *Ifnar1*$^{+/+}$ ("WT") and *Ifnar1*^{S526A} mice ("SA") were described previously (Bhattacharya et al., 2014). Other strains were generated by intercrossing and the littermates of 6-8 weeks of age were used in the experiments.

Cell Culture

Human and mouse cell lines such as human monocytic leukemia THP-1 cells (ATCC®TIB-202™), human 1205Lu melanoma (ATCC® CRL-2812™), and mouse B16F10 melanoma (ATCC® CRL-6475™) were purchased from ATCC and cultured according to the ATCC recommendations. Mouse mammary adenocarcinoma EO7771 cell line was purchased from CH3 Biosystems and cultured according to this provider's recommendations.

Human Samples

Informed consent was obtained from all study participants. Study approval was given by the Institutional Review Board of the University of Pittsburgh. Use of previously collected lymphocyte samples that could not be directly or indirectly linked to individual human subjects was conducted under the strict guidance of the institutional review at the University of Pittsburgh Medical Center.

METHOD DETAILS

Analysis of human samples. The cell surface IFNAR1 levels on lymphocytes from healthy donors or patients from two independent cohorts of melanoma patients were analyzed by flow cytometry. The MP1 cohort consisted of 40 patients with melanoma (stage I, II, III or IV). The MP2 cohort was described in details elsewhere (Tarhini et al., 2017)). These patients had a sentinel lymph node involved (SLN^{+}, n=20) or not (SLN^{-}, n=20) by melanoma metastasis as assessed by H&E and immunohistochemistry. Combined samples from patients from both cohorts (minus two patient samples lacking sufficient amount of material to extract RNA) were analyzed for *CH25H*.

Peripheral blood was aseptically collected into (green top) Na Heparin vacutainer tubes from healthy donors and melanoma patients. The blood was then stored at room temperature (16-30°C) and processed as follows. Whole blood was diluted (1:2) in PBS and gently mixed before adding 10 mL of Lymphocyte Separation media. The sample was centrifuged for 5 min at 1000 rpm and without stopping the speed was increased to 1800-2000 rpm for 20 min with the brake off. The peripheral blood leukocyte layer between the clear lymphocyte separation media and upper PBS layer was gently pipetted off.

The cells were washed with PBS three times and suspended in media (Iscov's Modified Dulbecco's Medium, 10% Human Serum, 1% Pen-Strep solution, 1% L-Glutamine, 1% MEM non-essential amino acids 10mM, 1% HEPES Buffer solution 1M) with 10% DMSO for incubation at -80°C overnight before long term storage at -140°C. For recovery, frozen cells were thawed rapidly (< 1 minute) in a 37°C water bath by gently swishing the tube in the water without submerging. The thawed cells were slowly, but immediately, transferred into 10 ml of PBS. The cells were twice washed with PBS before flow cytometry analyses or RNA extraction.

Blood samples were collected from patients with melanoma (n = 13) or healthy volunteers (n = 8) to isolate extracellular vesicles from plasma. Blood specimens were immediately processed by centrifugation at 1,000 x g for 10 min at room temperature and plasma was separated and frozen in aliquots at -80°C. Frozen plasma samples were thawed and centrifuged at 2,000 x g for 10 min at room temperature and at 14,000 x g for 30 min at 4°C for thrombocyte removal. Centrifuged plasma was applied to a 0.22 μm-pore Millipore filter. Extracellular vesicle isolation was performed on mini-size exclusion chromatography columns as previously described (Hong et al.,

2016). Briefly, plastic columns (Bio-Rad Econo-Pac columns, 1.5 cm x 12 cm) were packed with 10ml Sepharose 2B including a frit on top (Sigma-Aldrich, St. Louis, MO, USA) and washed with phosphate buffered saline (PBS). Clarified plasma (1mL) was loaded on top of the column and then eluted with 1mL PBS per fraction. Fraction 4 was used for further investigations. Detailed characterization of these extracellular vesicles is described elsewhere (Sharma et al., 2018).

Extracellular vesicles isolation from cell culture and labeling. The media from 80% confluent cells grown in Extracellular Vesicle-free (EV-free) was collected. The cancer cell extracellular vesicles were separated via ultracentrifugation as previously described (Thery et al., 2006). Extracellular vesicles were characterized in size and number by the Characterization Core Facility in the University of North Carolina at Chapel Hill while corresponding images were taken by Analytical and Nanofabrication Laboratory in the University of North Carolina at Chapel Hill using TEM JEOL 100CX II scope. Protein concentration was assessed using the Pierce BCA Protein Assay Kit. Extracellular vesicles were stored at -80°C for long term storage and thawed on ice before use. For labelling, extracellular vesicles were suspended in sterile PBS solution containing 5 µg/mL of the lipophilic dye DiD (Biotium Cat# 60014) dissolved in DMSO, incubated at 37°C for 10 min, transferred into ultracentrifugation tubes and washed twice with 35 mL of sterile PBS and re-suspended in PBS.

Plasma Membrane Profiling Proteomic Screen. Plasma Membrane Profiling uses selective aminooxy-biotinylation and quantitative proteomics to compare the expression of cell surface receptors in experimental and control cells, and was performed as previously described (Matheson et al., 2015; Weekes et al., 2012; Weekes et al., 2013; Weekes et al., 2014). Briefly, for Stable Isotope Labelling with Amino Acids in Cell Culture (SILAC)-based quantitation, THP-1 cells were pre-labeled for 7 days with light, medium or heavy isotopes of lysine and arginine (Cambridge Isotope Laboratories). Cells were then treated with either PBS or 1205Lu TEV (50 µg per $2x10^7$ cells for 2 hr), washed in ice-cold PBS and mixed in a 1:1 ratio. For aminooxy-biotinylation of plasma membrane proteins, cells were resuspended in a "one pot" aminooxy-biotinylation mix comprising 1mM sodium meta-periodate (Thermo Scientific), 100 µM aminooxy-biotin (Biotium) and 10mM aniline (Sigma) in ice-cold PBS pH 6.7 and incubated for 30 min in the dark. After lysis in 1% Triton X-100 (Thermo Scientific), biotinylated proteins were captured on High Capacity Streptavidin Agarose Resin (Thermo Scientific), stringently washed, reduced and alkylated prior to on-bead digestion with trypsin (Promega). Eluted peptides were subjected to LC–MS/MS using an RSLCnano 3000 (Thermo Scientific) coupled to a Q Exactive (Thermo Scientific). MS data were acquired from m/z 400 to 1650 with MS/MS spectra acquired in a top 10 DDA fashion. Raw MS files were processed using MaxQuant 1.5.0.0 and searched against a UniProt Homo sapiens database (downloaded 03/03/2014). Oxidation (M), deamidation (N/Q) and acetylation (Protein N-terminus) were set as variable modifications and carbamidomethyl (C) as a fixed modification. Peptide re-quantify was enabled and quantitation utilized razor and unique peptides. Parallel experiments were conducted in triplicate, including a three-way SILAC label swap (TEV/PBS, replicate 1: heavy/light; replicate 2: medium/heavy; replicate 3: light/medium). For each protein, TEV/PBS abundance ratios were compared using a one-sample t-test (XLSTAT) with theoretical mean log2(ratio)=0.

Isolation of primary mouse splenocytes, fibroblasts, bone marrow cells and peripheral blood leukocytes. Mice (3-5 week old) were euthanized and their spleens were immediately removed before forcibly traversed through a 70 µm cell strainer and washed with PBS. The samples were incubated with red blood cell lysis buffer and washed three times with PBS. The splenocytes were counted and seeded in suspension plates in complete media [RPMI with 10% EV-free FBS and 1:2000 dilution of cell culture grade β-mercaptoethanol] and allowed to rest for at least 4 hr and no more than 8 hr before experimental set up.

Lungs from these mice were aseptically removed, washed in ice-cold PBS, minced with a scalpel blade and incubated in dissociation solution (8 mL of 100 mg Collagenase II and 5 mg DnaseI in HBSS) at 37°C for 30-45 min. The collagenase reaction was quenched by diluting with equal volume of 100% EV-Free FBS. The dissociated tissue traversed a 100 µm cell strainer and the flow through was applied to a 40 µm cell strainer. The cells were washed twice with PBS before plating on a 15 cm tissue culture plate in antibiotic-free media (DMEM with 10% EV-free FBS). After 20-40 min, the non-adherent cells were removed; the remaining cells were washed thoroughly with PBS and left to rest in complete media (DMEM with 10% EV-Free FBS).

Bone marrow was flushed from femurs and tibia of these mice with PBS using 26 gauge needles. The cells were traversed a 70 µm cell strainer and then treated with red blood cell lysis buffer before washed and suspended in complete media (RPMI with 10% EV-Free FBS and 1:2000 dilution of cell culture grade β-mercaptoethanol). The bone marrow cells were seeded in suspension plates for immediate experimental use. Peripheral blood was aseptically collected from the mouse tail vein into (green top) Na Heparin capiject tubes. The blood samples were suspended in red blood cell lysis buffer and washed thoroughly with PBS prior to experimental use.

Cell treatment in vitro.25-Hydroxycholesterol was dissolved in 100% Ethanol to make a 4 mM working stock solution. Cells were washed with PBS to remove residual media and suspended in serum-free media containing 4 µM

of 25-Hydroxycholesterol. Reserpine and other drugs were dissolved in DMSO or water as indicated. For reserpine, a 100 µM stock solution was used. Cultured human and mouse cells were washed with PBS and suspended in complete media with 10 µM of Reserpine or DMSO alone for 2 hr.

For in vitro treatment with tumor derived extracellular vesicles, the cells were washed and counted to $1x10^6$ cells per mL and suspended in appropriate media with EV-free FBS. For each mL, 10 µg of B16F10 TEV added for mouse cells and 20 µg of 1205Lu TEV to human cells. A 2 hr incubation time point was used to measure changes in IFNAR1 cell surface level via flow cytometry. The 4 hr incubation time point was used to analyze TEV uptake and prepare samples for qPCR.

For IFN pretreatment, human cells were treated with 1000 U/mL of human IFNα or IFNβ for 12 hr and were then given 20 µg of labeled 1205Lu TEV for 4 hr. Cells were then thoroughly washed with PBS and suspended in PBS with DAPI for flow cytometry analysis. Freshly isolated mouse splenocytes and bone marrow cells were seeded in suspension plates at $1x10^6$ cells/mL and treated with 1000 U/mL with mouse IFNβ for 8 hr. The mouse cells were then treated with 10 µg of B16F10 TEV for 2 hr (with gentle mixing every 30 min) to examine changes in IFNAR1 level, or 4 hr to examine TEV uptake via flow cytometry.

Lung Tissue Dissociation for Flow Cytometry. Lung tissues were collected from euthanized mice and washed with ice cold PBS. The lung tissues are then cut into small pieces using sharp dissection scissors. The tissue homogenate is then incubated in dissociation solution (3 ml/lung) (dissociation solution: 2 mg/ml Collagenase II, 1 mg/ml Collagenase D plus 100 µg/ml Dnase I solution) for around 1 hr with continuous agitation at 37 degree. The digested tissue was passed through 70 µm cell strainer and the digestion quenched with 10 ml 10% FBS RPMI medium. The cells were centrifuged prior to incubation with RBC lysis buffer for 5 min to remove red blood cells. The cells are washed three times with PBS before prepped for flow cytometry experiments.

EV and liposomes uptake. ***For in vitro assays***, cells were washed and counted to $1x10^6$ cells per mL and re-suspended in appropriate media with EV-free FBS. For each mL, 10 µg of DiD-labeled B16F10 TEV for 4 hr or 1 µL of DiD-labeled liposomes were added for 2 hr. The cells were then washed thoroughly and analyzed by flow cytometry.

Short or long term experiments were used to analyze ***in vivo*** **TEV Uptake.** For short term experiments, 30 µg of DiD-labeled TEV were injected into the tail vein of 5 to 7 week old mice. Mice that received vehicle or Reserpine were injected 30 min prior to TEV tail vein injection. 24 hr after injection, the spleens and bone marrow were isolated from the euthanized mice for immediate analysis. For long term experiments, 8 µg of B16F10 TEV were injected into the tail veins of 5 to 7 week old mice three times a week for 3 weeks. Mice that received vehicle or reserpine were injected 30 min prior to each TEV tail vein injection. The tissues were collected 3 days after the final injection and splenocytes or bone marrow cells were analyzed by flow cytometry.

Cells that uptake EV and liposomes incorporate the DiD-dye into their plasma membranes, which allowed us to gate for DiD positive, DAPI negative cells using BD FACS Canto II (660/20 Red laser) or BD LSR Fortessa (670/30 Red laser) flow cytometers with BD FACS DIVA software. Comparison of DiD positivity was analyzed using FlowJo 10.4.1 (FlowJo, LLC, Ashland, OR).

For fluorescence, lungs collected from the bone marrow transfer recipients following survival surgery were cut in 8.0 µm sections onto glass slides. The sections were incubated in 1% paraformaldehyde in PBS for 3 min to fix tissue without quenching GFP and RFP signals. The tissues were washed four times with PBS before excess liquid removed and sections sealed with ProLong Gold Antifade Reagent with DAPI (Life Technologies) and glass coverslip.

For immunofluorescence, OCT stored tissues were cut into 8.0 µm sections onto glass slides and fixed in 100% acetone at -20°C for 10 min before allowed to dry at room temperature. The tissues were re-hydrated and washed with PBS. The samples were incubated in 0.2% Triton in PBS for 10 min at room temperature and washed 3 times in PBS before blocking in 5% Goat Serum in PBS. Tissue samples were incubated with primary antibodies overnight at 4°C and washed three times with PBS before incubated with respective secondary antibody at room temperature for 1 hr. ProLong Gold Antifade Reagent with DAPI was added. Non-confocal images were taken using the Olympus BX51 microscope. Confocal images were taken using Leica SP5-II FLIM.

For Flow Cytometry Analysis, cells were washed with PBS and incubated with human or mouse Fc block diluted in 0.5% BSA-PBS on ice for 10 min. Cells were then incubated with APC-conjugated anti-human CD45 antibody and anti-human AA3 IFNAR1 antibody (Goldman et al., 1999) 30 min on ice. FITC-anti-Rabbit Alexa Fluor antibody was added to bind AA3 for 30 min on ice. Cells were washed to remove unbound primary and secondary antibodies before suspended in PBS with DAPI for flow cytometry analysis on a LSR Fortessa (BD Biosciences) equipped with FACS DIVA software.

Mouse cells were washed with PBS and incubated with mouse Fc block diluted in 0.5% BSA-PBS. Afterward, cells were incubated with APC-conjugated anti-mouse CD45 and PE-conjugated anti-mouse IFNAR1. Cells were washed to remove unbound antibodies then suspended in PBS with DAPI for flow cytometry analysis on FACS Canto II and

LSR Fortessa (BD Biosciences) equipped with FACS DIVA. In all cases, the changes in mean fluorescence intensity (ΔMFI) was calculated as follows:

ΔMFI = Sample MFI – Control (IgG) MFI

Quantitative Real-Time PCR Analysis. Total RNA was isolated from samples using Trizol Reagent and chloroform. RNA concentration and purity was measured using a NanoDrop spectrophotometer. Applied Biosystems High-Capacity RNA-to-cDNA Kit was used to make cDNA. The mRNA expression levels were measured by quantitative real-time PCR using SYBR Green Master Mix.

For immunoprecipitation and immunoblot analysis, THP-1 cells were grown to no more than $2x10^6$ cells per mL with media changed every two days. Six hr before experiment, cells were seeded in suspension plates with fresh media. Cells treated with 1000 IU/mL of human IFNα-a2 or 20 μg/mL of 1205Lu TEV for 30 min or 2 hr with some gentle agitation every 30 min. The cells were transferred to pre-chilled conical tubes to remove media and wash cells with ice-cold PBS twice to removed media. The cell pellets were lysed using lysis buffer with protease and phosphatase inhibitors as previously described. Protein concentration detected using the Pierce BCA Protein Assay Kit. For immunoprecipitation, 1mg of lysate was pre-cleared with Protein A/G beads for one hour prior to overnight incubation with anti-IFNAR1 (EA12) antibody (Goldman et al., 1999) with fresh Protein A/G beads. The supernatant removed and the beads were washed four times with 1xTBS with 0.001% Tween-20. The beads were then boiled in 4xSDS loading dye with β-mercaptoethanol for 10 min at 98°C. The whole cell lysates and immunoprecipitation samples were separated on SDS PAGE, transferred onto PVDF membranes and analyzed as previously described (Bhattacharya et al., 2013; Bhattacharya et al., 2014).

Generating Bone Marrow Chimeric Animals. 5 week old mice were injected with 10 μg of B16F10 TEV or PBS into the tail vein three times a week for four weeks. The mice were euthanized and the bone marrow cells were flushed with PBS from the long bones. Recipient mice were irradiated with 900 rads and allowed to rest for 3 hr before injected with 500,000 bone marrow cells through the tail vein. The mice were given 4-6 weeks to recover post transplantation before being inoculated with B16F10 tumors followed by analysis of primary tumor growth and metastases.

In Vivo Subcutaneous Tumor Growth. B16F10 cells at 60-70% confluence were lifted off the plate using 2mM EDTA in PBS. The lifted cells were washed with PBS and suspended in fresh PBS to $1x10^6$ cells per 100 μL. The cells were kept on ice and 100 μL were injected subcutaneously into the flanks of mice. Tumors were measured every other day and resected when tumor volume reached approximately 200 mm2.

Reserpine Adjuvant Treatment. Mice with s.c. B16F10 tumors that were approximately 30-50 mm^2, began pre-surgical treatment with reserpine (1 mg/kg dissolved in ascorbic acid and diluted in ddH_2O) or vehicle (0.1% ascorbic acid diluted in ddH2O) three times (every other day) for one week. Once the tumor reaches approximately 200 mm^2, the tumors were resected. One week after surgery or upon healed sutures, the animals began weekly treatment with reserpine (or vehicle). When animals displayed signs of respiratory stress or became moribund, they were sacrificed and their lungs were analyzed for metastatic lesions.

Collection of Lungs for frozen sections or H&E. Mice were euthanized and the lungs were gently perfused with ice cold PBS to wash out blood and prevent tissue collapse. For H&E analysis, the lungs were then perfused with 4% paraformaldehyde solution before processed for paraffin embedding. For fluorescence and immunofluorescence analysis, PBS perfused lungs were then perfused with 50% OCT solution before freezing in 100% OCT for cryosections.

Analysis of Tumor Number and Size in Lung Tissue. The Leica DM6000 widefield microscope was used to take low magnification images to generate composite images of whole, H&E stained lungs. The composite images were opened in ImageJ to accentuate tumor-rich areas, remove background noise, and define size of neoplasm. Composite images of H&E stained primary tumor were used as controls to set ImageJ parameters. ImageJ then creates a mask that was superimposed to the original H&E pictures to verify areas that contained cancer cells. The ImageJ mask was then analyzed to count number of nodules and also to calculate area of lung with tumor burden.

QUANTIFICATION AND STATISTICAL ANALYSIS

All described results are representative of at least three independent experiments ($n \geq 5$ mice per group in each experiment unless specified otherwise). All in vitro analyses using cells or tissues from each of these animals were done at least in biological triplicates (e.g. samples from 3 tumors, 3 spleens, etc). Data are presented as average ± S.E.M. Statistical analysis was performed using Microsoft Excel (Microsoft) or GraphPad Prism 7 software (GraphPad Prism Software Inc). For analysis of proteomics data, For each protein, TEV/PBS abundance ratios were compared using a one-sample t-test (XLSTAT) with theoretical mean log2(ratio)=0. Unpaired Student t test was used for the comparison between two groups. One-way ANOVA or two-way ANOVA analysis followed by the Bonferroni post-hoc test were used for the multiple comparisons. Repeated-measure two-way ANOVA (mixed-

model) followed by the Bonferroni post-hoc test was used for the analysis of tumor growth curve. The Kaplan-Meier curves were used to depict the survival function from lifetime data for mice and human patients; the Peto's log-rank test was used to estimate the differences between the groups. The Student *t*-test or Fisher test were used for other comparisons. A value of $p < 0.05$ was considered significant.

KEY RESOURCES TABLE

REAGENT or RESOURCE	SOURCE	IDENTIFIER
Antibodies		
Mouse monoclonal anti-phospho p38(T180/Y182) (28B10)	Cell Signaling	Cat#9216S
Rabbit monoclonal anti-phospho p38(T180/Y182) (28B10)	Cell Signaling	Cat#4631S
Rabbit monoclonal anti-phospho STAT1(Y701) (58D6)	Cell Signaling	Cat# 9167S
Rabbit monoclonal anti-STAT1 (9H2)	Cell Signaling	Cat#9176S
Rabbit monoclonal anti-βTRCP (D13F10)	Cell Signaling	Cat#4394S
Rabbit monoclonal anti-GAPDH (D16H11)	Cell Signaling	Cat#5174S
Rabbit monoclonal anti-β-Tubulin	Cell Signaling	Cat#2146S
Rabbit monoclonal anti- p38 (N-20)	Santa Cruz	Cat#SC-728
Rat monoclonal anti-CD11b unconjugated (clone M1/70)	BioLegend	Cat#101202
Mouse monoclonal anti-IFNAR1-PE (clone MAR1-5A3)	BioLegend	Cat#127311
Mouse monoclonal anti-CD11b-FITC (clone M1/70)	BioLegend	Cat#101205
Mouse monoclonal anti-CD45-APC (clone 30-F11)	BioLegend	Cat#103112
Mouse monoclonal anti-Ubiquitin (FK2)	Millipore Sigma	Cat#ST1200
Rabbit monoclonal anti-human IFNAR1	Abcam	Cat#ab45172
Rabbit polyclonal anti-Fibronectin	Abcam	Cat#23750
Rabbit polyclonal anti-IFNAR1	Sinobiological	Cat#50469-RP02
mouse IgG	Leinco Technologies	cat# I-536
Mouse monoclonal anti-mouse IFNAR1 (clone MAR1-5A3)	Leinco Technologies	cat# I-401
Mouse monoclonal anti-human IFNAR1 (clone AA3)	(Goldman et al., 1999)	N/A
Mouse monoclonal anti-human IFNAR1 (clone EA12)	(Goldman et al., 1999)	N/A
Rabbit polyclonal anti-phosphoSer-IFNAR1	(Bhattacharya et al., 2010; Bhattacharya et al., 2011)	N/A
Biological Samples		
Human extracellular vesicles	This paper and (Sharma et al., 2018)	N/A
Human leukocytes	This paper and (Tarhini et al., 2017)	N/A
Chemicals, Peptides, and Recombinant Proteins		
25-hydroxycholesterol	Sigma-Aldrich	Cat# H1015 CAS#2140-46-7
Reserpine	Sigma-Aldrich	Cat#83580 CAS#50-55-5
Simvastatin	Sigma-Aldrich	Cat#S6196 CAS#79902-63-9
Roglitone	Sigma-Aldrich	Cat#R2408 CAS#122320-73-4
Toremifene	Sigma-Aldrich	Cat#T7204 CAS#89778-27-8
Enclomiphene	Sigma-Aldrich	Cat#SML0719 CAS#14158-65-7
Trifluoperazine	Sigma-Aldrich	Cat#T8516 CAS#79902-63-9
Simvastatin	Sigma-Aldrich	Cat#S6196 CAS#440-17-5
Latex beads, fluorescent yellow-green	Sigma-Aldrich	Cat#L5155

LY294002 (p38 inhibitor)	Selleckchem	Cat# S1494 CAS# 862507-23-1
Recombinant mouse IFNβ	PBL Assay	Cat#12401-1
Human IFNβ (1a)	PBL Assay	Cat# 11415-1
human IFNα (2a)	PBL Assay	Cat#11100-1
Recombinant mouse IFNγ	BioLegend	Cat#575306
DiD lipophilic dye	Biotium	Cat# 60014 CAS#127274-91-3
DiD-labeled Liposomes (100 nanometers)	FormuMax Liposome Reagents	Cat#F60103F
Collagenase II	MP Biomedicals	Cat#1005002 CAS#9001-12-1
Collagenase D	Roche Diagnostics	Cat#11088882001
DNaseI, grade II	Roche Diagnostics	Cat#10104159001
Critical Commercial Assays		
Power Sybr Green PCR Master Mix	Applied Biosystems	Cat#4367659
High-Capacity cDNA Reverse Transcription Kit	Applied Biosystems	Cat#4368814
Pierce BCA Protein Assay Kit	ThermoFisher	Cat#23225
Experimental Models: Cell Lines		
Human: THP-1 monocytic leukemia	ATCC	Cat# TIB-202
Human: 1205Lu melanoma	ATCC	Cat# CRL-2812
Mouse: B16F10 melanoma	ATCC	Cat# CRL-6475
Mouse: EO771 mammary adenocarcinoma	CH3 Biosystems	Cat#940001
Experimental Models: Organisms/Strains		
Mouse WT C57BL/6	The Jackson Laboratory	Cat#000664
Mouse: C57BL/6 *Ch25h*$^{-/-}$	The Jackson Laboratory	Cat#016263
Mouse: C57BL/6 *Ifnar1*^{S526A}	(Bhattacharya et al., 2014; Yu et al., 2015)	N/A
Mouse: C57BL/6 *Ifnar1*^{S526A};*Ch25h*$^{-/-}$	This paper	N/A
Mouse: C57BL/6 *Mapk14*$^{f/f}$*; Ubc9-CreERT*	(Katlinski et al., 2017)	N/A
Oligonucleotides		
Primers for qPCR and genotyping, see Table S3	This paper	N/A
Software and Algorithms		
FlowJo software version 10	FlowJo Software	https://www.flowjo.com/
GraphPad Prism software	GraphPad Software	http://www.graphpad.com
Microsoft Excel 2010	Microsoft Office	N/A

Figure 1

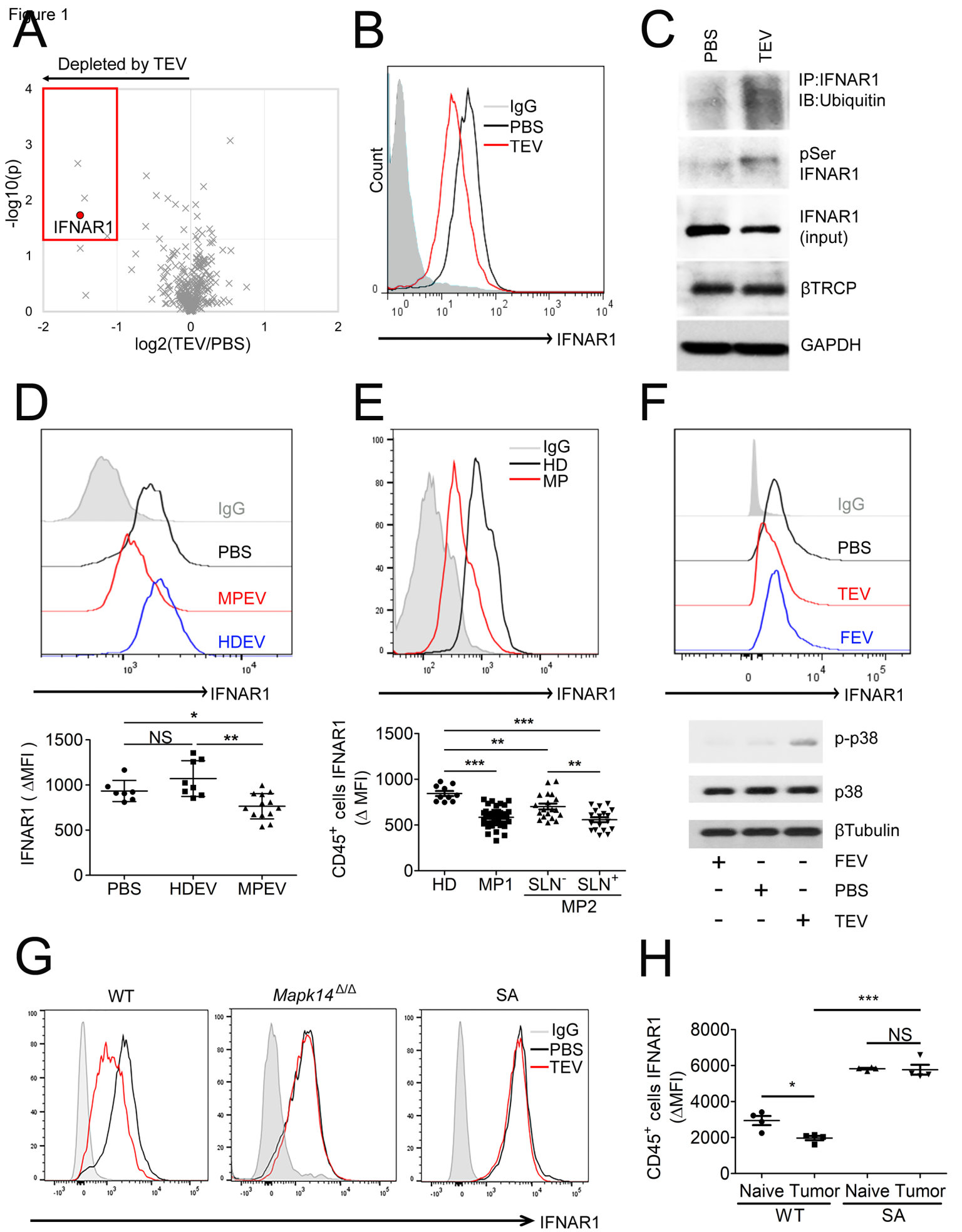
A
Depleted by TEV
-log10(p)
IFNAR1
log2(TEV/PBS)
B
IgG
PBS
TEV
Count
IFNAR1
C
PBS
TEV
IP:IFNAR1
IB:Ubiquitin
pSer
IFNAR1
IFNAR1
(input)
βTRCP
GAPDH
D
IgG
PBS
MPEV
HDEV
IFNAR1
IFNAR1 (ΔMFI)
NS
PBS
HDEV
MPEV
E
IgG
HD
MP
IFNAR1
CD45+ cells IFNAR1
(Δ MFI)
HD
MP1
SLN-
SLN+
MP2
F
IgG
PBS
TEV
FEV
IFNAR1
p-p38
p38
βTubulin
FEV
PBS
TEV
G
WT
Mapk14Δ/Δ
SA
IgG
PBS
TEV
IFNAR1
H
CD45+ cells IFNAR1
(ΔMFI)
NS
Naive
Tumor
Naive
Tumor
WT
SA

Figure 2

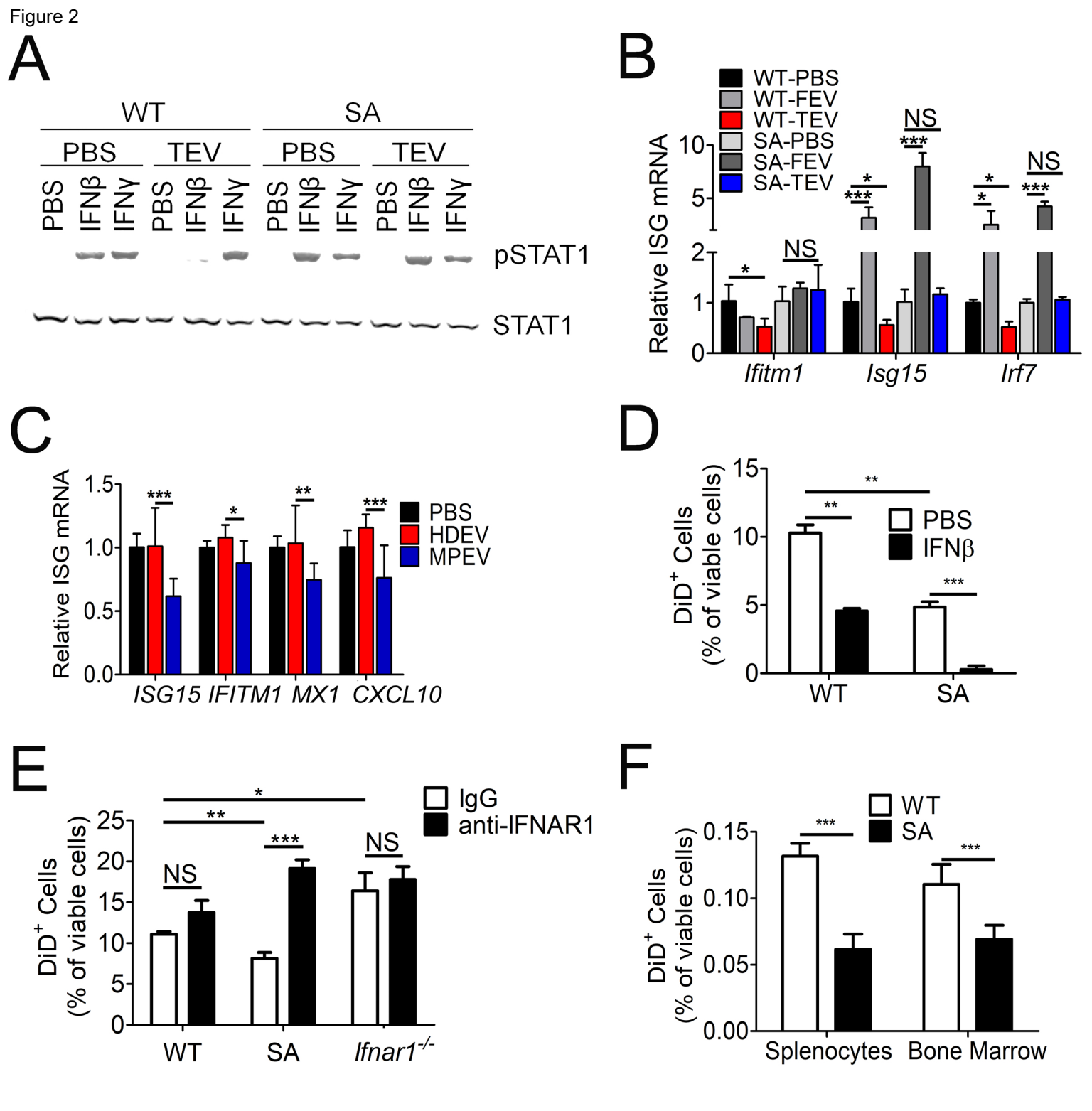
A
WT
SA
PBS
TEV
PBS
IFNβ
IFNγ
pSTAT1
STAT1
B
WT-PBS
WT-FEV
WT-TEV
SA-PBS
SA-FEV
SA-TEV
Relative ISG mRNA
Ifitm1
Isg15
Irf7
NS
C
Relative ISG mRNA
PBS
HDEV
MPEV
ISG15
IFITM1
MX1
CXCL10
D
DiD+ Cells
(% of viable cells)
PBS
IFNβ
WT
SA
E
DiD+ Cells
(% of viable cells)
IgG
anti-IFNAR1
WT
SA
Ifnar1-/-
F
DiD+ Cells
(% of viable cells)
WT
SA
Splenocytes
Bone Marrow

Figure 3

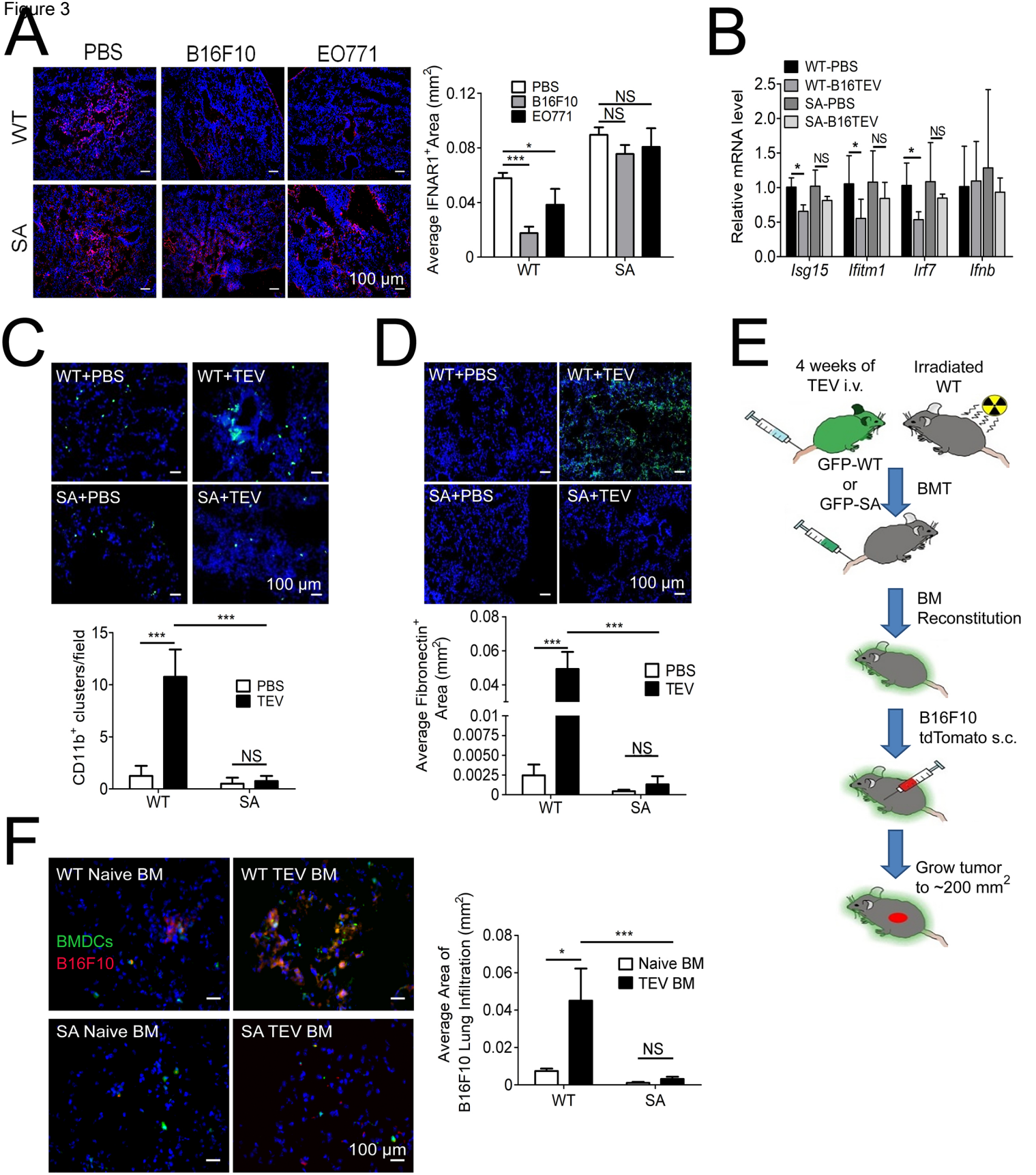
A
PBS
B16F10
EO771
WT
SA
100 μm
Average IFNAR1+Area (mm2)
PBS
B16F10
EO771
NS
*
***
WT
SA
B
WT-PBS
WT-B16TEV
SA-PBS
SA-B16TEV
Relative mRNA level
Isg15
Ifitm1
Irf7
Ifnb
C
WT+PBS
WT+TEV
SA+PBS
SA+TEV
100 μm
CD11b+ clusters/field
PBS
TEV
D
Average Fibronectin+ Area (mm2)
E
4 weeks of TEV i.v.
Irradiated WT
GFP-WT or GFP-SA
BMT
BM Reconstitution
B16F10 tdTomato s.c.
Grow tumor to ~200 mm2
F
WT Naive BM
WT TEV BM
SA Naive BM
SA TEV BM
BMDCs
B16F10
Average Area of B16F10 Lung Infiltration (mm2)
Naive BM
TEV BM

Figure 4

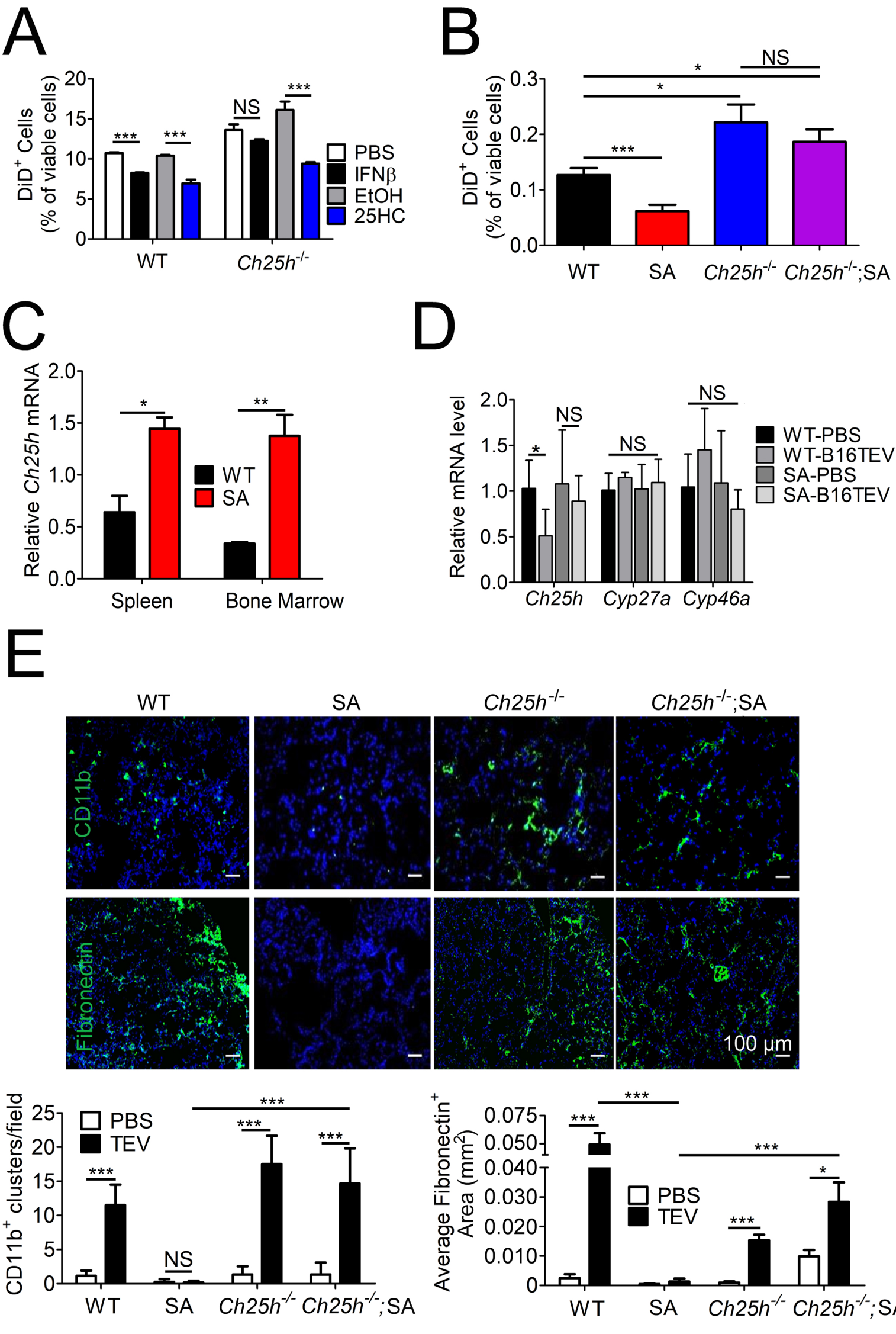
A
DiD+ Cells (% of viable cells)
PBS
IFNβ
EtOH
25HC
WT
Ch25h-/-
B
DiD+ Cells (% of viable cells)
NS
WT
SA
Ch25h-/-
Ch25h-/-;SA
C
Relative Ch25h mRNA
WT
SA
Spleen
Bone Marrow
D
Relative mRNA level
NS
WT-PBS
WT-B16TEV
SA-PBS
SA-B16TEV
Ch25h
Cyp27a
Cyp46a
E
WT
SA
Ch25h-/-
Ch25h-/-;SA
CD11b
Fibronectin
100 μm
CD11b+ clusters/field
PBS
TEV
Average Fibronectin+ Area (mm2)

Figure 5

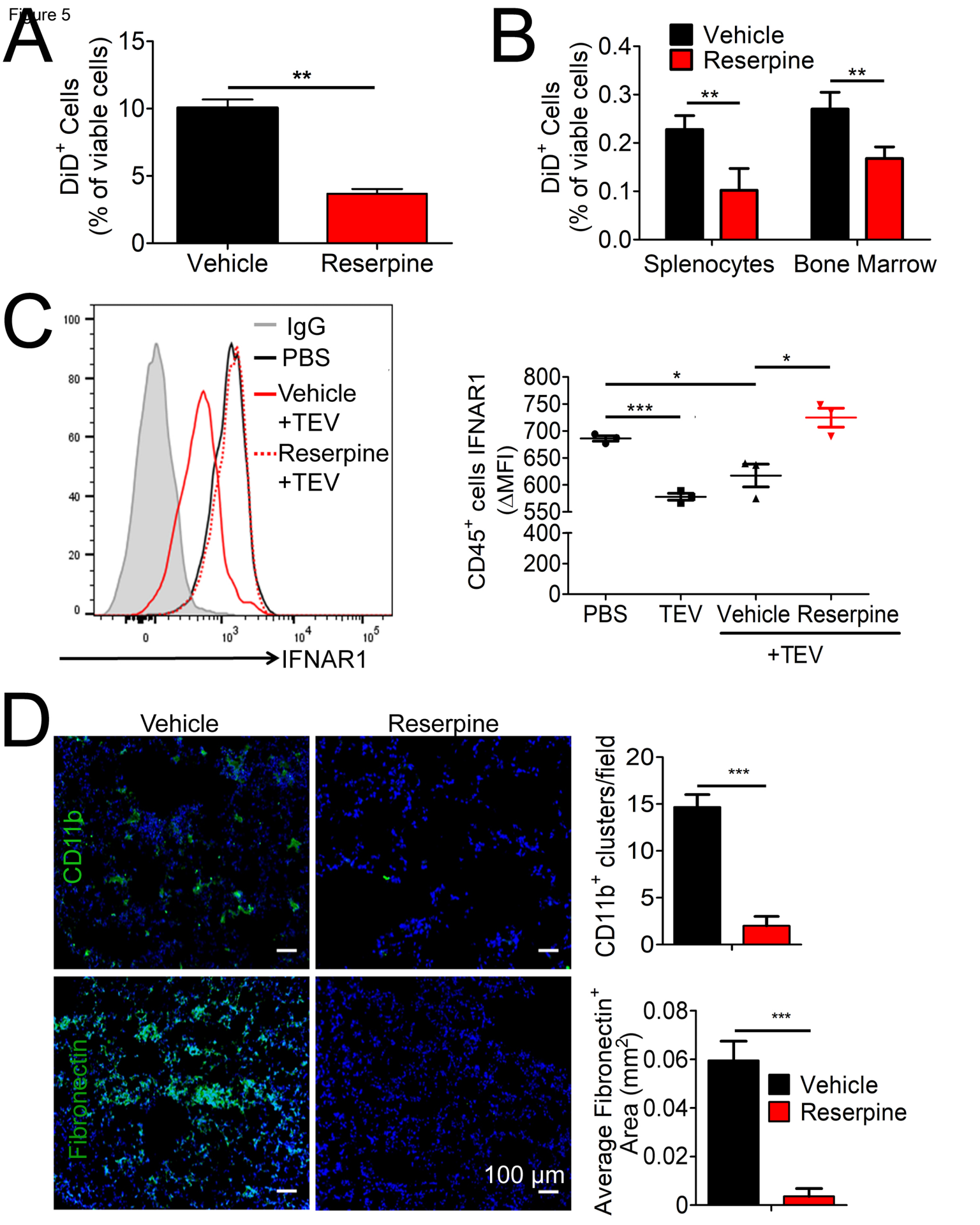
A
DiD+ Cells (% of viable cells)
15
10
5
0
**
Vehicle
Reserpine
B
Vehicle
Reserpine
DiD+ Cells (% of viable cells)
0.4
0.3
0.2
0.1
0.0
**
**
Splenocytes
Bone Marrow
C
IgG
PBS
Vehicle +TEV
Reserpine +TEV
100
80
60
40
20
0
0
10^3
10^4
10^5
IFNAR1
CD45+ cells IFNAR1 (ΔMFI)
800
750
700
650
600
550
400
200
0
*
*
***
PBS
TEV
Vehicle
Reserpine
+TEV
D
Vehicle
Reserpine
CD11b
Fibronectin
100 μm
CD11b+ clusters/field
20
15
10
5
0
***
Average Fibronectin+ Area (mm2)
0.08
0.06
0.04
0.02
0
***
Vehicle
Reserpine

Figure 6

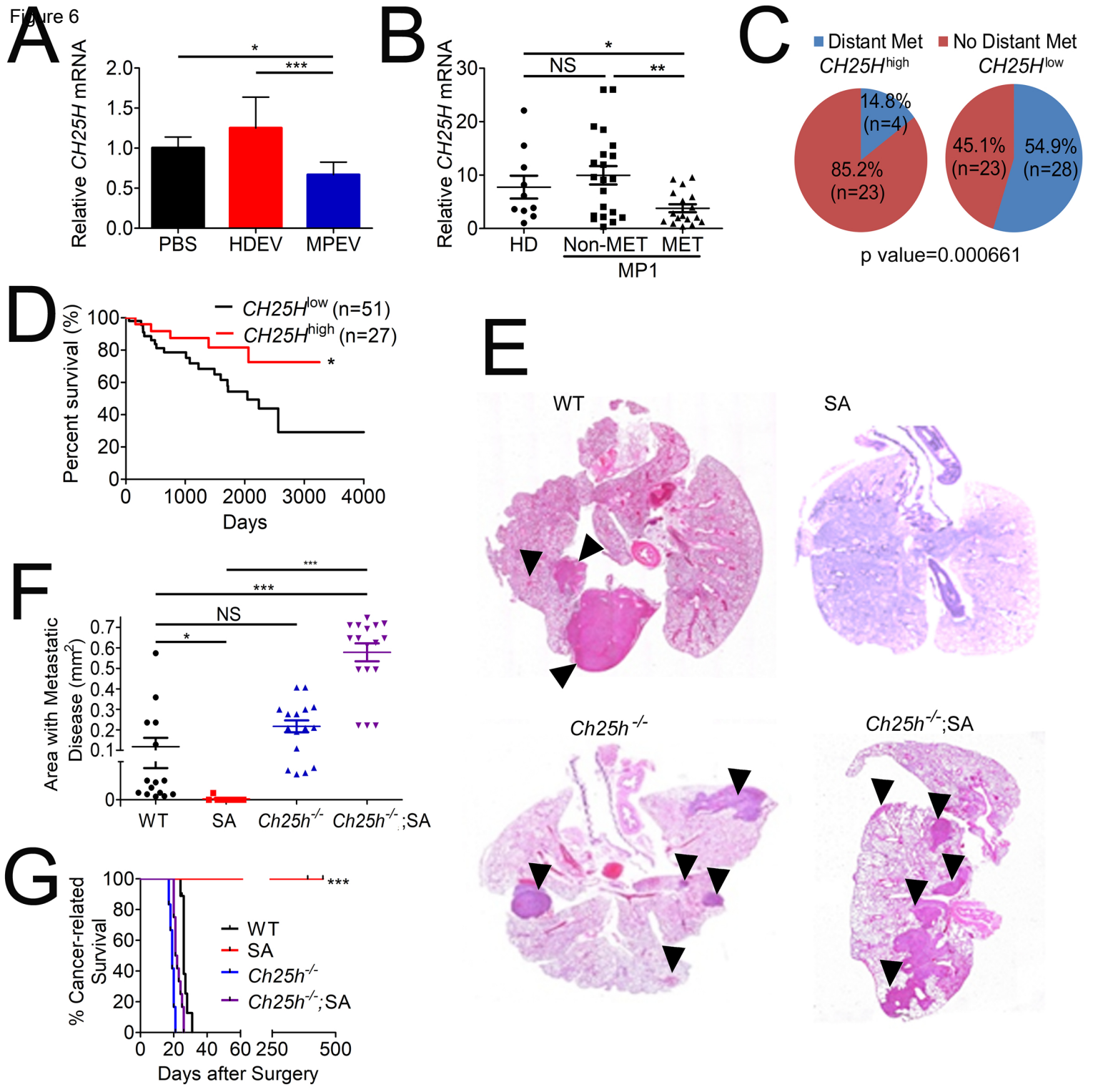
A
Relative CH25H mRNA
2.0
1.5
1.0
0.5
0.0
*
***
PBS
HDEV
MPEV
B
Relative CH25H mRNA
30
20
10
0
*
NS
**
HD
Non-MET
MET
MP1
C
Distant Met
No Distant Met
CH25Hhigh
CH25Hlow
14.8%
(n=4)
85.2%
(n=23)
45.1%
(n=23)
54.9%
(n=28)
p value=0.000661
D
Percent survival (%)
100
80
60
40
20
0
CH25Hlow (n=51)
CH25Hhigh (n=27)
*
0
1000
2000
3000
4000
Days
E
WT
SA
Ch25h-/-
Ch25h-/-;SA
F
Area with Metastatic Disease (mm2)
0.7
0.6
0.5
0.4
0.3
0.2
0.1
0
***
***
NS
*
WT
SA
Ch25h-/-
Ch25h-/-;SA
G
% Cancer-related Survival
100
80
60
40
20
0
***
WT
SA
Ch25h-/-
Ch25h-/-;SA
0
20
40
60
250
500
Days after Surgery

Figure 7

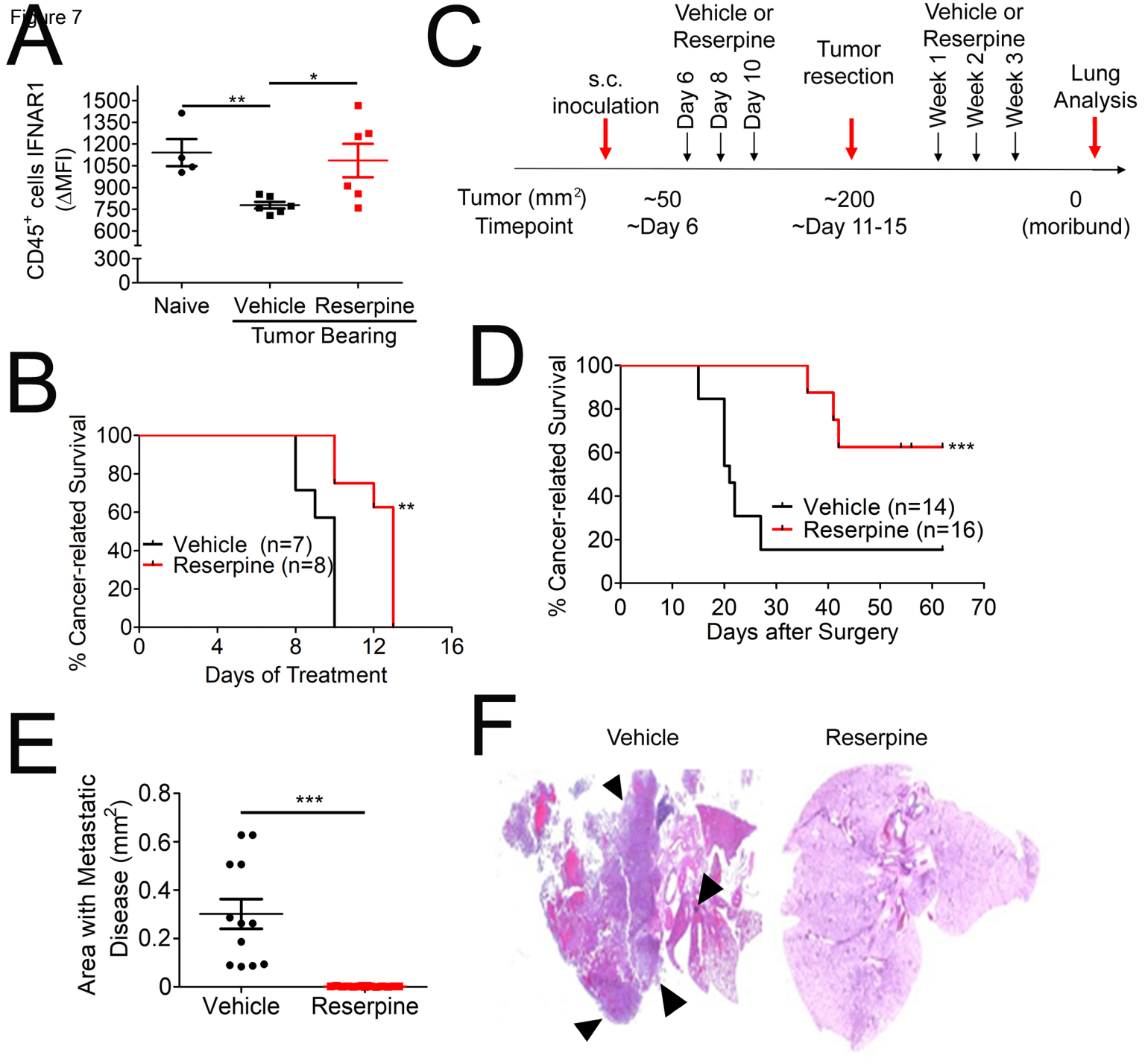
A
CD45+ cells IFNAR1 (ΔMFI)
1500
1350
1200
1050
900
750
600
300
0
**
*
Naive
Vehicle
Reserpine
Tumor Bearing
C
s.c. inoculation
Vehicle or Reserpine
Day 6
Day 8
Day 10
Tumor resection
Vehicle or Reserpine
Week 1
Week 2
Week 3
Lung Analysis
Tumor (mm2)
Timepoint
~50
~Day 6
~200
~Day 11-15
0
(moribund)
B
% Cancer-related Survival
100
80
60
40
20
0
0
4
8
12
16
Days of Treatment
Vehicle (n=7)
Reserpine (n=8)
**
D
% Cancer-related Survival
100
80
60
40
20
0
0
10
20
30
40
50
60
70
Days after Surgery
Vehicle (n=14)
Reserpine (n=16)
***
E
Area with Metastatic Disease (mm2)
0.8
0.6
0.4
0.2
0
***
Vehicle
Reserpine
F
Vehicle
Reserpine

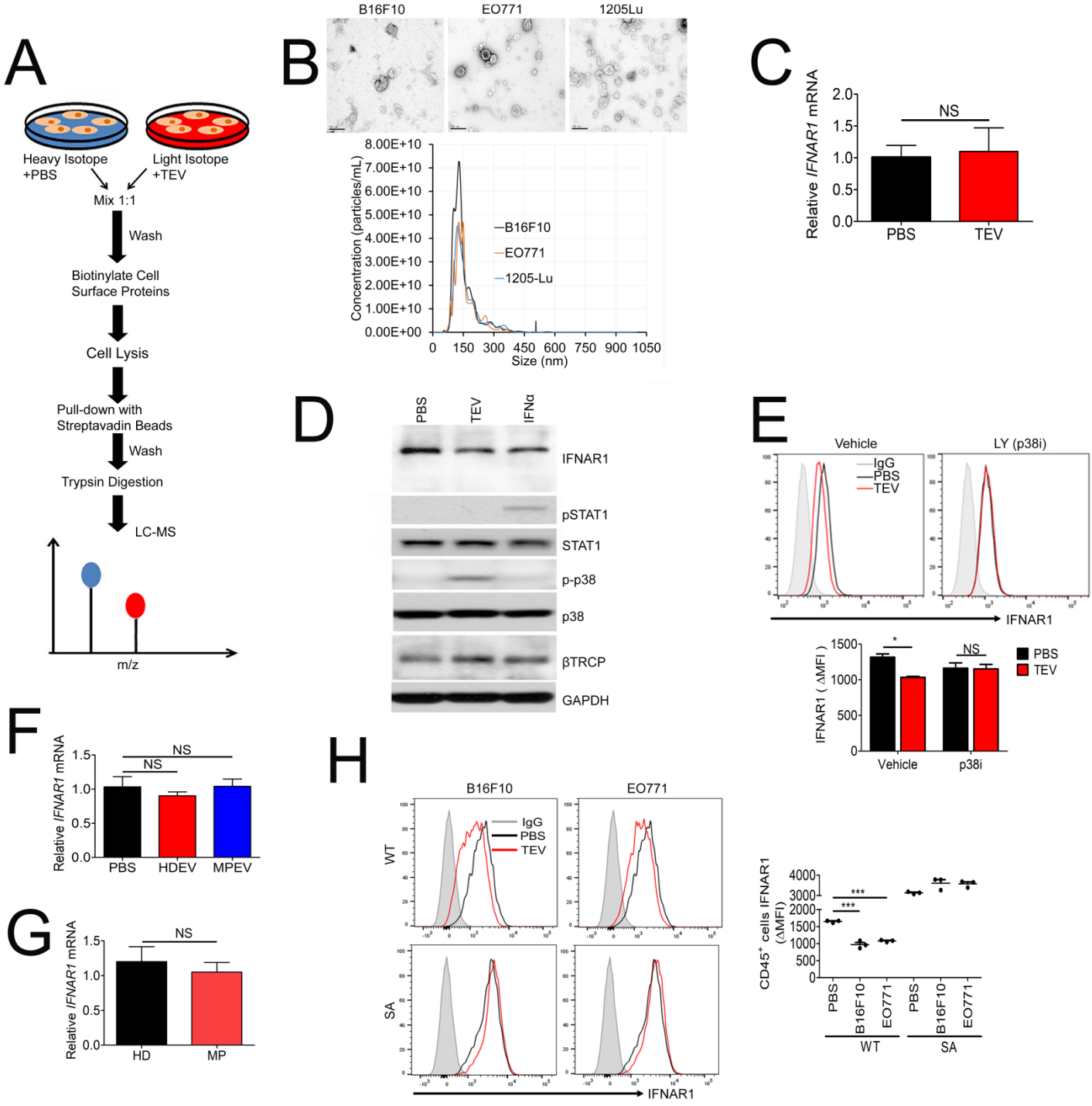

Figure S1, related to Figure 1

A. Schematic for SILAC-based Plasma Membrane Profiling screen to analyze TEV-mediated alterations in cell surface protein levels. These experiments were conducted in triplicate, with a three-way SILAC label swap.

B. Characterization of TEV. Top Panel: Transmission Electron Microscopy images of TEV derived from 1205Lu, B16F10, and EO771 cell lines (scale bar 200nm); Bottom Panel: Nanoparticle Tracking Analysis comparing size distribution of TEV from different cell lines (1205Lu, B16F10, and EO771).

C. qPCR analysis of *IFNAR1* mRNA levels in THP-1 cells treated with PBS or 1205Lu TEV.

D. Effect of TEV (10 μg/10^6 cells for 2 hr) or human IFNα (1000 IU/mL for 2 hr) treatment on the phosphorylation and total levels of indicated proteins in THP-1 cells analyzed by immunoblot.

E. Flow analysis of IFNAR1 surface levels on THP-1 cells pretreated with vehicle or p38 inhibitor LY294002 (2 μM for 1 hr) prior to treatment with PBS or 1205Lu TEV (2 hr). Representative histogram (top) and MFI quantification (bottom) are shown.

F. qPCR analysis of *IFNAR1* mRNA levels in THP-1 cells treated with PBS, or extracellular vesicles derived from plasma of healthy donors (HDEV) or of melanoma patients (MPEV) as in Figure 1D

G. qPCR analysis of *IFNAR1* mRNA levels in peripheral blood lymphocytes from healthy donors (HD) or melanoma patients (MP) from two independent cohorts: MP1 (40 patients of different stages I-IV) and MP2 (20 patients in each of two groups that were positive (SLN^+) or negative (SLN^-) for sentinel lymph node metastases)

H. IFNAR1 levels on peripheral blood leukocytes isolated from WT and SA mice after i.v. treatment with TEV from B16F10 melanoma or EO771 mammary adenocarcinoma cells (8 μg, 3x per week for 3 weeks) or PBS. Representative histograms (left) and ΔMFI analyses (right) are shown.

Quantitative data are represented as mean ± SEM; p values: * $p<0.05$; ** $p<0.01$; *** $p<0.001$ from Student's t test (panels C, E, F, H).

Table S1, related to Figure 1

Plasma membrane proteins affected by melanoma TEV

Protein IDs	Protein names	Genes	TEV/CONa	TEV/CONb	TEV/CONc	Mean	Unique peptides
Q9H7F0; C9J7Z7	Probable cation-transporting ATPase 13A3	ATP13A3	-1.443320449	-1.478764767	-1.67337551	-1.531820242	25
B4DNT3;P17181; C9JV08; C9J114	Interferon alpha/beta receptor 1	IFNAR1	-1.904224076	-1.214062619	-1.38758312	-1.501956605	6
P20333; B5A977	Tumor necrosis factor receptor superfamily member 1B; Tumor necrosis factor-binding protein 2	TNFRSF1B;TNFR1B	-1.898134813	-1.956019469	-0.642378113	-1.498844132	2
P41231	P2Y purinoceptor 2	P2RY2	-1.325575507	-1.279827839	-1.716112942	-1.440505429	3
Q8NB49;H7C0E8	Probable phospholipid-transporting ATPase IG	ATP11C	0.646992084	-4.994489214	0.07553521	-1.423987307	5
P07333; E9PEK4	Macrophage colony-stimulating factor 1 receptor	CSF1R	-1.476618706	-1.262373019	-0.656908183	-1.131966636	3
E9PH29; P30048	Thioredoxin-dependent peroxide reductase, mitochondrial	PRDX3	-0.760993085	-1.497637911	-0.145873062	-0.801501353	3
Q9NPR2;J3KNP4;H0YMZ3;H0YMR1;H0YLN3;H0YNM2;H0YMD6;H0YKP2;H0YN49	Semaphorin-4B	SEMA4B	-1.072816539	-0.893983426	-0.270827916	-0.74587596	4
O95185; E0CX15; D6RE16; Q8IZJ1	Netrin receptor UNC5C	UNC5C	-0.396270408	-0.71228762	-0.722728309	-0.610428779	17

Q96F46	Interleukin-17 receptor A	IL17RA	-0.535206287	-0.608241513	-0.660381035	-0.601276278	8
P11021	78 kDa glucose-regulated protein	HSPA5	-0.351645007	-0.023184369	0.071967056	-0.100954107	4
Q8TDW0	Leucine-rich repeat-containing protein 8C	LRRC8C	-0.344190246	0.133653784	0.049501724	-0.053678246	5
Q8NBJ4;F8WAT9;C9JYM4	Golgi membrane protein 1	GOLM1	-0.083217651	0.169079469	-0.146785541	-0.020307908	4
F5GZY0;Q06481;F5H845;E9PQS3;E9PSC7	Amyloid-like protein 2	APLP2	-0.376002075	0.092186375	0.326009476	0.014064592	4
P40939;H0YFD6;B4DYP2	Trifunctional enzyme subunit alpha, mitochondrial;Long-chain enoyl-CoA hydratase;Long chain 3-hydroxyacyl-CoA dehydrogenase	HADHA	0.103396924	0.200431876	0.066865524	0.123564775	4
F5H7A2;O00592;F5GWY5	Podocalyxin	PODXL	0.221815228	0.187197865	0.025588164	0.144867086	4
P62937;F8WE65;C9J5S7;Q567Q0;Q9Y536;F5H284	Peptidyl-prolyl cis-trans isomerase A	PPIA	1.00122577	-1.337882322	1.411732707	0.358358718	3
P35408	Prostaglandin E2 receptor EP4 subtype	PTGER4	0.53037044	0.511608391	0.564798144	0.535592325	3
P11169;B7Z844;Q8TDB8;B7ZAC3;F5GYR5	Solute carrier family 2, facilitated glucose transporter member 3;Solute carrier family 2, facilitated glucose transporter member 14	SLC2A3;SLC2A14	0.221072783	0.7576231	0.657741106	0.545478996	6

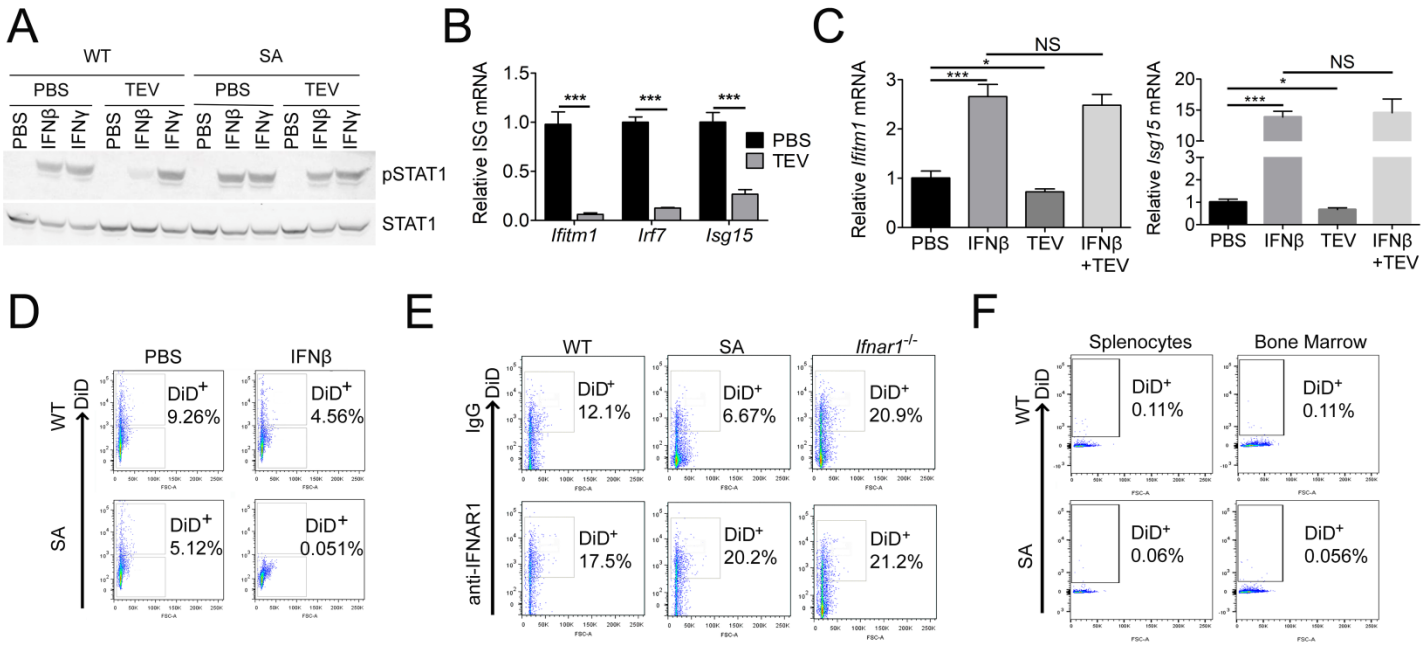
A
WT
SA
PBS
TEV
PBS
IFNβ
IFNγ
pSTAT1
STAT1
B
Relative ISG mRNA
PBS
TEV
Ifitm1
Irf7
Isg15
C
Relative Ifitm1 mRNA
Relative Isg15 mRNA
NS
PBS
IFNβ
TEV
IFNβ +TEV
D
PBS
IFNβ
WT
SA
DiD
DiD+ 9.26%
DiD+ 4.56%
DiD+ 5.12%
DiD+ 0.051%
E
WT
SA
Ifnar1-/-
IgG
anti-IFNAR1
DiD+ 12.1%
DiD+ 6.67%
DiD+ 20.9%
DiD+ 17.5%
DiD+ 20.2%
DiD+ 21.2%
F
Splenocytes
Bone Marrow
DiD+ 0.11%
DiD+ 0.11%
DiD+ 0.06%
DiD+ 0.056%

Figure S2, related to Figure 2

A. Effect of pre-treatment with TEV (10 μg per 10^6 cells for 90 min) on activation of STAT1 by IFNβ (250 IU/mL for 30 min) or IFNγ (50 IU/mL for 30 min) in indicated mouse embryo fibroblasts analyzed by immunoblotting.

B. qPCR analysis of mRNA for indicated genes in mouse splenocytes at 24 hr after they received multiple B16F10 TEV treatments (at t=2, 4, 6, 8, 10, 12, 14, 16, and 22 hr, 10 μg each).

C. qPCR analysis of mRNA for indicated genes in mouse splenocytes treated with IFNβ (1000 IU/mL for 8 hr), TEV (10 μg for 4 hr), or pre-treated with IFNβ followed by TEV as indicated.

D. Flow cytometry analysis of WT or SA splenocytes pre-treated with PBS or mouse IFNβ (1000 IU/mL for 8 hr treated with DiD-labeled B16F10 TEV (10 μg for 4 hr)

E. Flow cytometry analysis of uptake of DiD-labeled TEV (10 μg for 4 hr) by splenocytes from WT, SA or *Ifnar1*$^{-/-}$ mice pre-treated with IgG or the IFNAR1 neutralizing antibody MAR1-5A3 (30 ng/mL for 1 hr) as indicated

F. Flow cytometry analysis of DiD^+ splenocytes and bone marrow cells isolated from mice of indicated genotypes 24 hr after i.v. administration of DiD-labeled B16F10 (30 μg)

Quantitative data are represented as mean ± SEM; p values: * $p<0.05$; ** $p<0.01$; *** $p<0.001$ from Student's t test (panels B, C).

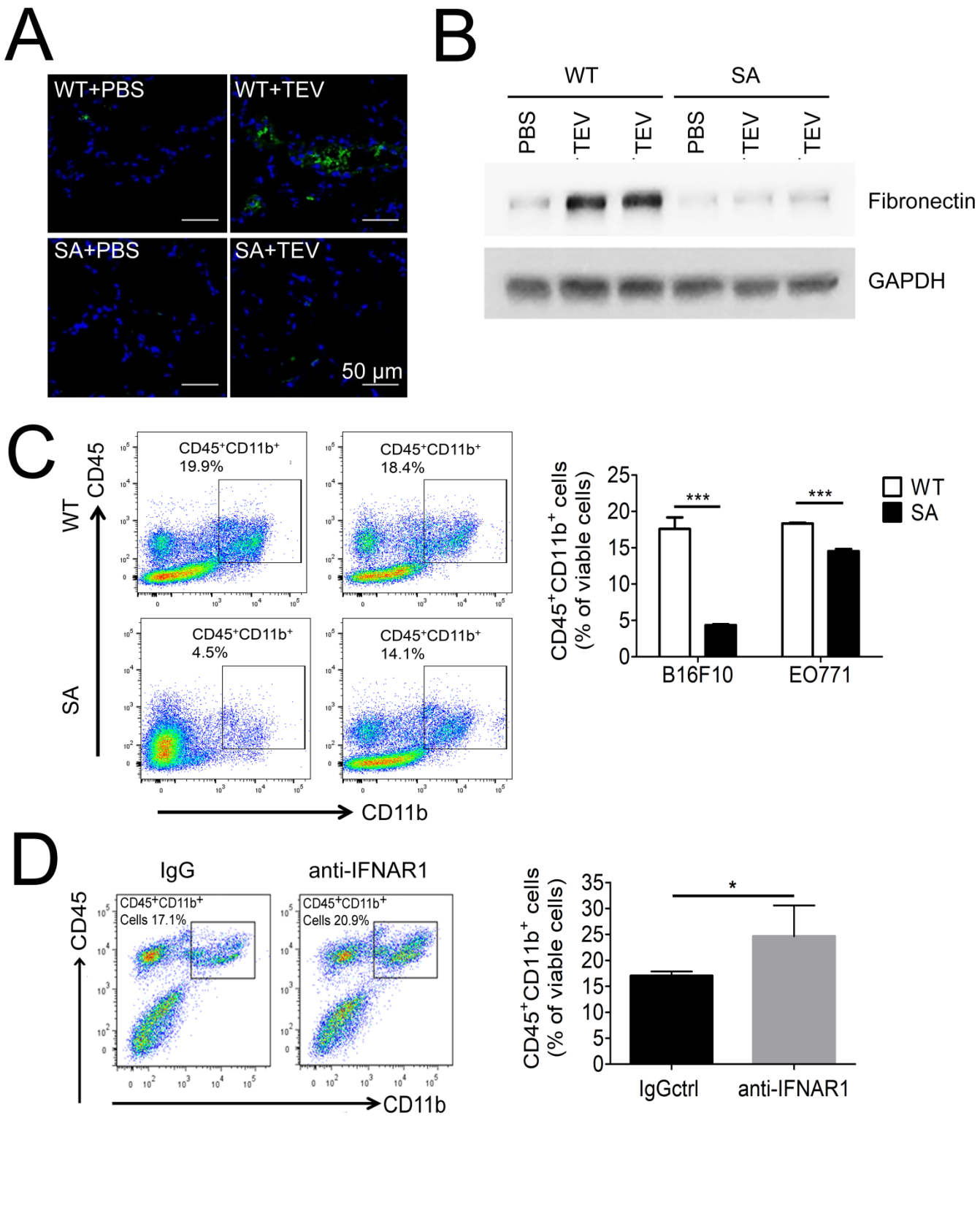
A
WT+PBS
WT+TEV
SA+PBS
SA+TEV
50 μm
B
WT
SA
PBS
TEV
TEV
PBS
TEV
TEV
Fibronectin
GAPDH
C
WT
SA
CD45
CD11b
CD45+CD11b+
19.9%
CD45+CD11b+
18.4%
CD45+CD11b+
4.5%
CD45+CD11b+
14.1%
CD45+CD11b+ cells
(% of viable cells)
***
***
WT
SA
B16F10
EO771
D
IgG
anti-IFNAR1
CD45
CD11b
CD45+CD11b+
Cells 17.1%
CD45+CD11b+
Cells 20.9%
CD45+CD11b+ cells
(% of viable cells)
*
IgGctrl
anti-IFNAR1

Figure S3, related to Figure 3

A. Immunofluorescence analysis of $CD11b^+$ clusters in the lungs of WT and SA animals treated with PBS or B16F10 TEV (i.v., 8 μg 3x per week for 3 weeks) as in Figure 3C. Scale bar - 50 μm.

B. Immunoblot analysis of fibronectin levels in the lungs of indicated mice that received PBS or B16F10 TEV for 3 weeks as described in Figure 3D. Levels of GAPDH serve as a loading control.

C. Flow cytometry analysis of $CD45^+CD11b^+$ cells in the lungs of WT and SA mice administered with TEV (i.v., 8 μg 3x per week for 3 weeks) isolated from indicated cancer cells; quantification of flow cytometry results as % of total lung cells is shown in the bottom panel

D. Flow cytometry analysis of $CD45^+CD11b^+$ cell infiltration in the lungs of SA animals treated with B16F10 TEV (i.v., 8 μg 3x per week for 3 weeks) and with control IgG or anti-IFNAR1 neutralizing antibody (1 mg/mouse i.p. every 5 days); quantification of flow cytometry results as % of total lung cells is shown in the bottom panel

Quantitative data are represented as mean ± SEM; p values: * $p<0.05$; ** $p<0.01$; *** $p<0.001$ from Student's t test (panels C, D)

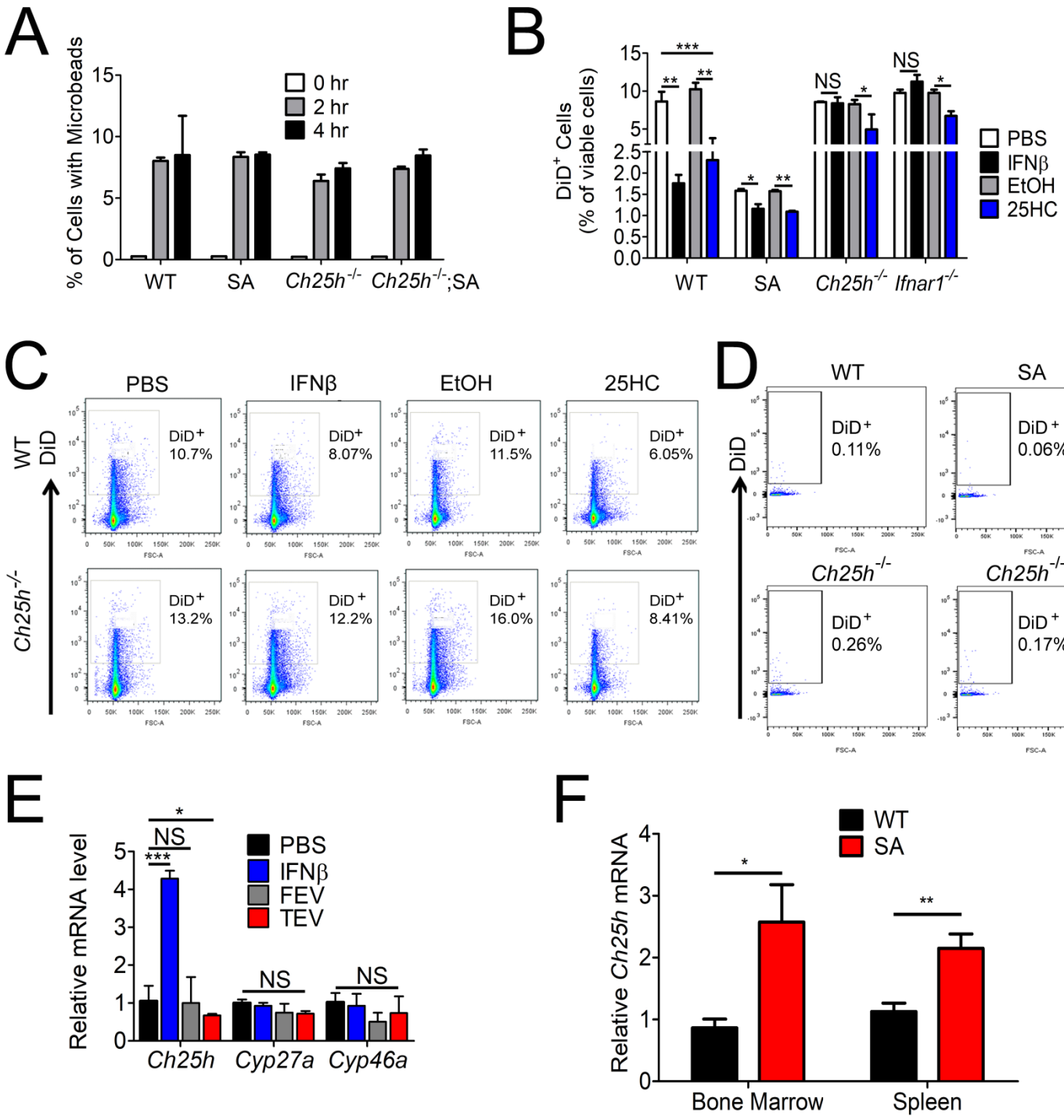
A
% of Cells with Microbeads
0 hr
2 hr
4 hr
WT
SA
Ch25h-/-
Ch25h-/-;SA
B
DiD+ Cells (% of viable cells)
PBS
IFNβ
EtOH
25HC
WT
SA
Ch25h-/-
Ifnar1-/-
C
PBS
IFNβ
EtOH
25HC
WT DiD
Ch25h-/-
DiD+ 10.7%
DiD+ 8.07%
DiD+ 11.5%
DiD+ 6.05%
DiD+ 13.2%
DiD+ 12.2%
DiD+ 16.0%
DiD+ 8.41%
FSC-A
D
WT
SA
Ch25h-/-
Ch25h-/-;SA
DiD
DiD+ 0.11%
DiD+ 0.06%
DiD+ 0.26%
DiD+ 0.17%
FSC-A
E
Relative mRNA level
PBS
IFNβ
FEV
TEV
Ch25h
Cyp27a
Cyp46a
F
Relative Ch25h mRNA
WT
SA
Bone Marrow
Spleen

Figure S4, related to Figure 4

A. Analysis of phagocytosis of fluorescent-labeled 0.1 μm beads by bone marrow macrophages from mice of indicated genotypes incubated with these beads for 0, 2 or 4 hr

B. Primary lung fibroblasts of indicated genotypes were pre-treated with IFNβ (1000 U/mL for 8 hr) or 25HCe (4 μM for 2 hr) and then incubated with DiD-labeled liposomes (1 μL, 2 hr). Quantification of uptake of liposomes is shown as % of DiD^+ cells.

C. Flow cytometry analysis of uptake of DiD-labeled B16F10 TEV by splenocytes from indicated mice pre-treated with PBS, IFNβ (1000 U/mL for 8 hr), ethanol (EtOH), or 25HC (4 μM for 2 hr)

D. Flow cytometry analysis of uptake of DiD-positive B16F10 TEV by splenocytes isolated from mice of indicated genotypes 24 hr after i.v. administration of DiD-labeled B16F10 (30 μg)

E. qPCR analysis of relative mRNA levels of *Ch25h* and other genes encoding cholesterol monooxygenases (*Cyp27a* and *Cyp46a*) in mouse splenocytes treated in vitro with PBS, IFNβ (1000 IU/ml, 8 hr), or extracellular vesicles (10 μg for 4hr) isolated from primary mouse lung fibroblasts (FEV), or B16F10 melanoma cells (TEV).

F. qPCR analysis of relative mRNA levels of *Ch25h* in indicated tissues isolated from naive WT and SA mice (n=4 each)

Quantitative data are represented as mean ± SEM; p values: * $p<0.05$; ** $p<0.01$; *** $p<0.001$ from Student's t test (panels A, B, E, F).

Table S2, related to Figure 5

Clinically relevant small molecule drugs reported to inhibit processes that involve lipid membrane fusion utilized in a mini-screen for suppression of TEV uptake

Compound	Known clinical use	Inhibitor of
Simvastatin	treatment of dyslipidemia and prevention of cardiovascular disease	osteoclast precursor fusion
Rosiglitazone	anti-diabetic of the thiazolidinedione class	osteoclast precursor fusion
Arbidol	licensed to treat acute respiratory infections	viral membrane fusion
Toremifene and Enclomiphene	selective estrogen receptor modulators	viral membrane fusion
Trifluoperazine	antipsychotic of the phenothiazine class	myoblast fusion
Reserpine	antihypertensive and antipsychotic agent	vesicular type inhibitor of neuromediator reuptake

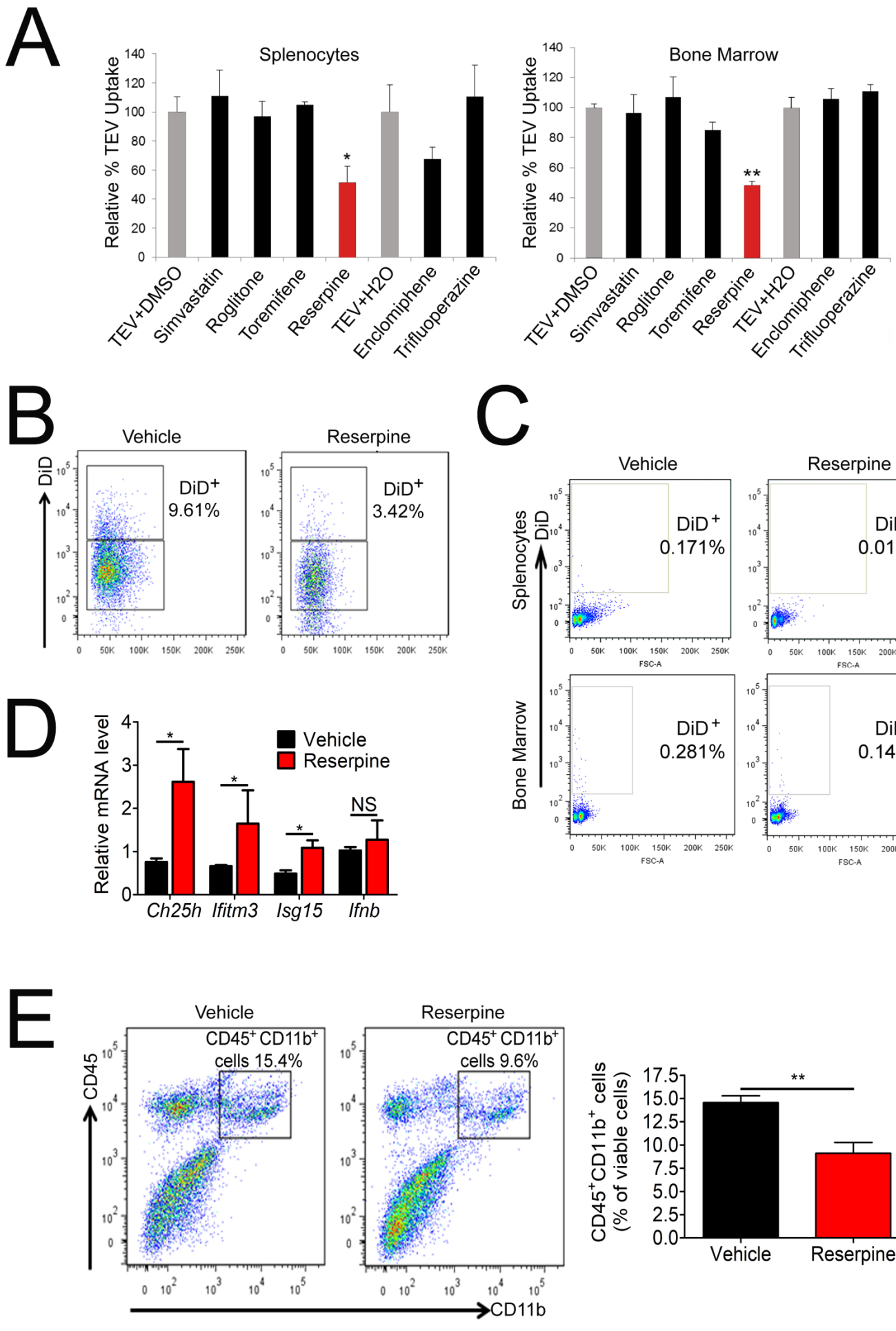
A
Splenocytes
Relative % TEV Uptake
140
120
100
80
60
40
20
0
*
TEV+DMSO
Simvastatin
Roglitone
Toremifene
Reserpine
TEV+H2O
Enclomiphene
Trifluoperazine
Bone Marrow
**
B
Vehicle
Reserpine
DiD
DiD+ 9.61%
DiD+ 3.42%
C
Vehicle
Reserpine
Splenocytes
Bone Marrow
DiD
DiD+ 0.171%
DiD+ 0.010%
DiD+ 0.281%
DiD+ 0.142%
FSC-A
D
Relative mRNA level
Vehicle
Reserpine
NS
Ch25h
Ifitm3
Isg15
Ifnb
E
Vehicle
Reserpine
CD45+ CD11b+ cells 15.4%
CD45+ CD11b+ cells 9.6%
CD45
CD11b
CD45+CD11b+ cells (% of viable cells)
17.5
15.0
12.5
10.0
7.5
5.0
2.5
0.0
**
Vehicle
Reserpine

Figure S5, related to Figure 5

A. Relative uptake of TEV by primary mouse splenocytes or bone marrow cells pre-treated with indicated inhibitors (10 μM for 2 hr) following by incubation with B16F10 DiD-labeled TEV (10 μg/10^6 cells, 4 hr) from melanoma cells calculated as % of uptake of cell pre-treated with appropriate vehicles (DMSO for simvastatin, rogliton, toremifene and reserpine and H_20 for enclomiphene and trifluoroperazine).

B. Flow cytometry analysis of DiD^+ THP-1 cells treated as in Figure 5A.

C. Flow cytometry analysis of DiD^+ splenocytes and bone marrow cells isolated from WT mice 24 hr after i.p. injection of vehicle or reserpine (1 μg/kg i.p., given 30 min before TEV injection) followed by i.v. administration of DiD-labeled B16F10 (30 μg) as in Figure 5b

D. qPCR analysis of indicated gene expression in bone marrow from WT mice receiving i.p. vehicle or reserpine treatment followed by i.v. treatment with B16F10TEV (8 μg, 3x per week for 3 weeks)

E. Flow cytometry analysis of myeloid ($CD45^+CD11b^+$) cell infiltration in the lungs from WT mice receiving i.p. vehicle or reserpine and TEV treatment (as in Figure 5D).

Quantitative data are represented as mean ± SEM; p values: * $p<0.05$; ** $p<0.01$; *** $p<0.001$ from Student's t test (panels A, D, E).

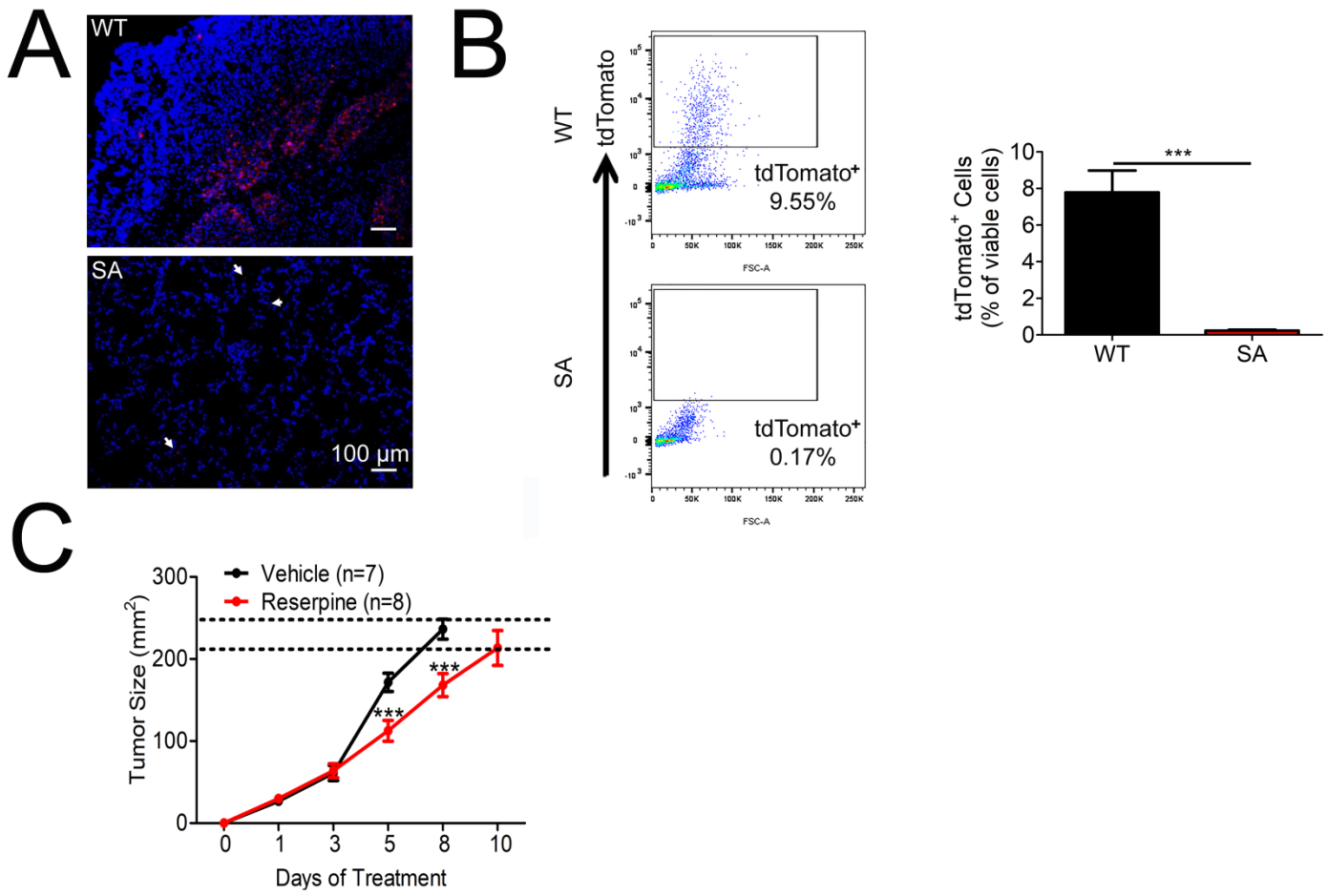
A
WT
SA
100 μm
B
WT
SA
tdTomato
tdTomato+
9.55%
tdTomato+
0.17%
FSC-A
tdTomato+ Cells
(% of viable cells)
***
WT
SA
C
Vehicle (n=7)
Reserpine (n=8)
Tumor Size (mm2)
Days of Treatment
***
***

Figure S6, related to Figure 6

A. Immunofluorescence analysis of lungs of WT and SA mice sacrificed 60 days after surgical removal of s.c. ~200mm^2 TdTomato$^+$ expressing B16F10 tumors

B. Flow analysis (left panel) and quantification (right panel) of the TdTomato$^+$ B16F10 cells from the lungs of mice described in panel A (n=3 for each group)

C. Growth of primary B16F10 tumors inoculated s.c. at 1x10^6 cells in mice of indicated genotypes until the tumors reached the size of surgical resection (~200 mm^2).

Quantitative data are represented as mean ± SEM; p values: * $p<0.05$; ** $p<0.01$; *** $p<0.001$ from Student's t test (panel B) or Anova test (panel C).

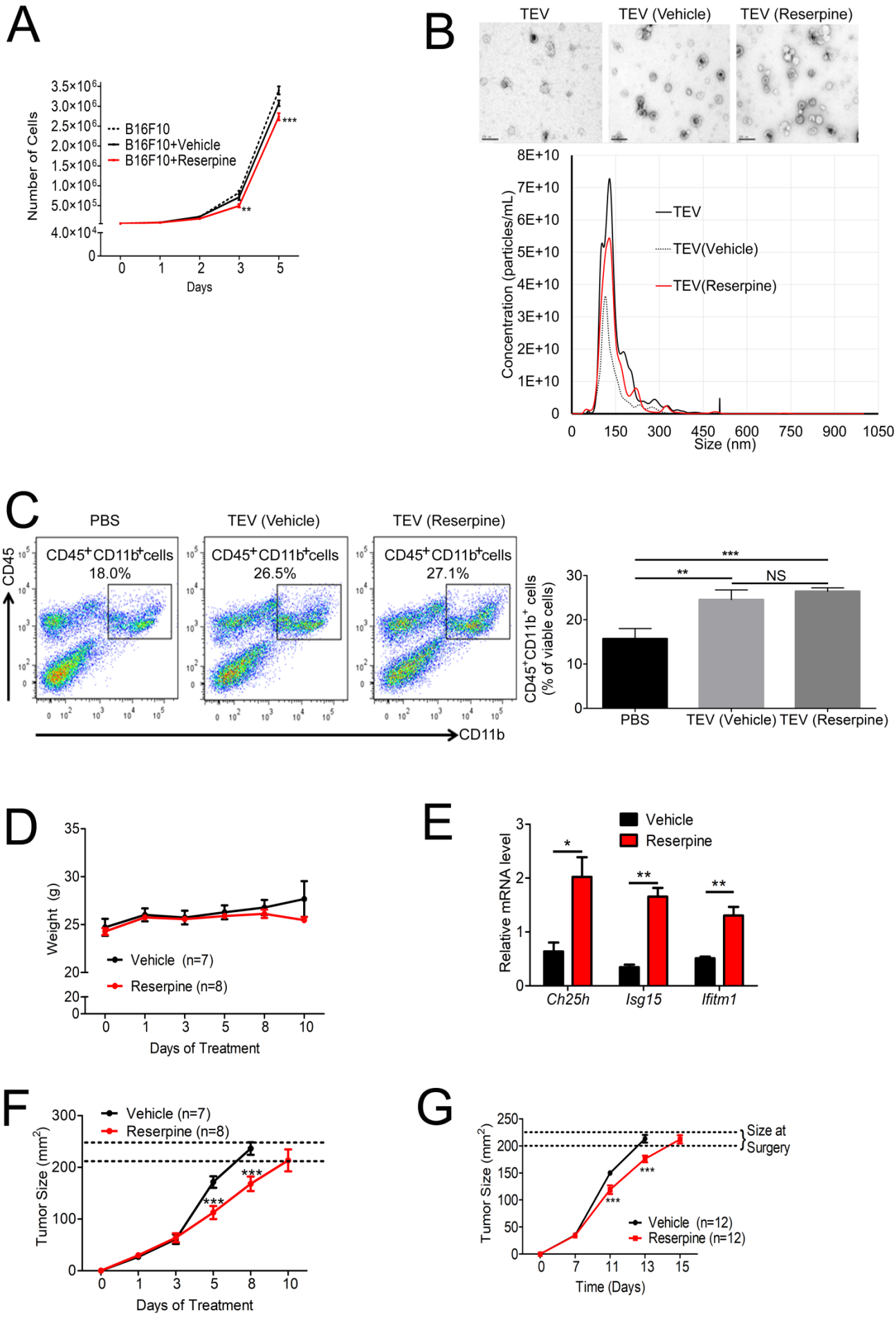
A
Number of Cells
B16F10
B16F10+Vehicle
B16F10+Reserpine
Days
B
TEV
TEV (Vehicle)
TEV (Reserpine)
Concentration (particles/mL)
TEV
TEV(Vehicle)
TEV(Reserpine)
Size (nm)
C
PBS
TEV (Vehicle)
TEV (Reserpine)
CD45
CD45+CD11b+cells 18.0%
CD45+CD11b+cells 26.5%
CD45+CD11b+cells 27.1%
CD11b
CD45+CD11b+ cells (% of viable cells)
NS
D
Weight (g)
Vehicle (n=7)
Reserpine (n=8)
Days of Treatment
E
Vehicle
Reserpine
Relative mRNA level
Ch25h
Isg15
Ifitm1
F
Vehicle (n=7)
Reserpine (n=8)
Tumor Size (mm2)
Days of Treatment
G
Size at Surgery
Tumor Size (mm2)
Vehicle (n=12)
Reserpine (n=12)
Time (Days)

Figure S7, related to Figure 7

A. In vitro proliferation of B16F10 cells (untreated or treated with vehicle or reserpine at 10 μM).

B. Transmission Electron Microscopy images of TEVs isolated from B16F10 cells cultured untreated or in the presence of vehicle or reserpine (10 μM for 5 days). The nanoparticle tracking analysis of TEV size distribution from these cells following is shown in the bottom panel.

C. Flow cytometry analysis of $CD45^{+}CD11b^{+}$ cell infiltration of the lungs of WT animals treated with PBS or TEV (i.v., 8 μg 3x per week for 3 weeks) isolated from B16F10 cells treated in vitro with vehicle or reserpine (10 μM for 5 days). Quantification is shown in the bottom panel.

D. Body weights of B16F10 tumor bearing WT animals treated with vehicle or reserpine (i.p. 1 mg/kg every 48 hr for 1 week)

E. qPCR analysis of indicated gene expression in the lungs from B16F10 tumor-bearing WT mice receiving i.p. vehicle or reserpine treatment as in panel d.

F. Growth of primary B16F10 tumors inoculated s.c. at $1x10^6$ cells in WT animals treated with vehicle or reserpine (i.p. 1 mg/kg every 48 hr for 1 week)

G. Growth B16F10 tumors inoculated s.c. at $1x10^5$ cells in WT animals treated with vehicle or reserpine (i.p. 1 mg/kg, 3x per week for 1 week) until reaching indicated size

Quantitative data are represented as mean ± SEM; p values: * $p<0.05$; ** $p<0.01$; *** $p<0.001$ from Student's t test (panels A, C, E) or Anova test (panels D, F, G).

Table S3, related to STAR methods

List of oligonucleotides used for qPCR or mouse genotyping

REAGENT or RESOURCE	SOURCE	IDENTIFIER
Oligonucleotides for qPCR		
Primer: Human *ISG15* Forward GAGCATCCTGGTGAGGAATAAC	Sigma-Aldrich	N/A
Primer: Human *ISG15* Reverse CGCTCACTTGCTGCTTCA	Sigma-Aldrich	N/A
Primer: Human *IFITM1* Forward TCTCAGAGGAGCCTGGCTAA	Sigma-Aldrich	N/A
Primer: Human *IFITM1* Reverse CCAGACTATCCTTGACCTGATGA	Sigma-Aldrich	N/A
Primer: Human *MX1* Forward CTTTCCAGTCCAGCTCGGCA	Sigma-Aldrich	N/A
Primer: Human *MX1* Reverse AGCTGCTGGCCGTACGTCTG	Sigma-Aldrich	N/A
Primer: Human *CXCL10* Forward AGCTCTACTGAGGTGCTATGT	Sigma-Aldrich	N/A
Primer: Human *CXCL10* Reverse GTACCCTTGGAAGATGGGAAAG	Sigma-Aldrich	N/A
Primer: Human *CH25H* Forward GCTACTCTTCGACATGGAGTTC	Sigma-Aldrich	N/A
Primer: Human *CH25H* Reverse CAGTTCCCAGACGCTCATATAC	Sigma-Aldrich	N/A
Primer: Mouse *Isg15*Forward GGAACGAAAGGGGCCACAGCA	Sigma-Aldrich	N/A
Primer: Mouse *Isg15* Reverse CCTCCATGGGCCTTCCCTCGA	Sigma-Aldrich	N/A
Primer: Mouse *Ifitm1* Forward ATCTCCACGCCTGACCATGT	Sigma-Aldrich	N/A
Primer: Mouse *Ifitm1* Reverse CACCCACCATCTTCCTGTCC	Sigma-Aldrich	N/A
Primer: Mouse *Ifitm3* Forward CTGCTGCCTGGGCTTCATAG	Sigma-Aldrich	N/A
Primer: Mouse *Ifitm3* Reverse GGATGCTGAGGACCAAGGTG	Sigma-Aldrich	N/A
Primer: Mouse *Mx1* Forward CTCACCTCCCACATCTGTAAATC	Sigma-Aldrich	N/A
Primer: Mouse *Mx1* Reverse GTATGTCTGCACCGTACTTCTG	Sigma-Aldrich	N/A
Primer: Mouse *Ch25h* Forward TGCTACAACGGTTCGGAGC	Sigma-Aldrich	N/A
Primer: Mouse *Ch25h* Reverse AGAAGCCCACGTAAGTGATGAT	Sigma-Aldrich	N/A
Primer: Mouse *Cyp46a1* Forward CCTTCTTCATTGCTGGTCACG	Sigma-Aldrich	N/A
Primer: Mouse *Cyp46a1*Reverse TCCATCACTGTGAACGCCAAG	Sigma-Aldrich	N/A
Primer: Mouse *Cyp27a1* Forward CCAGGCACAGGAGAGTACG	Sigma-Aldrich	N/A
Primer: Mouse *Cyp27a1* Reverse GGGCAAGTGCAGCACATAG	Sigma-Aldrich	N/A
Primer: human *GAPDH* Forward AGGGCTGCTTTTAACTCTGGT	Sigma-Aldrich	N/A
Primer: Human *GAPDH* Reverse CCCCACTTGATTTTGGAGGGA	Sigma-Aldrich	N/A

Primer: Mouse *Gapdh* Forward AGCTTGTCATCAACGGGAAG	Sigma-Aldrich	N/A
Primer: Mouse *Gapdh* Reverse TTTGATGTTAGTGGGGTCTCG	Sigma-Aldrich	N/A
Oligonucleotides (PCR) for genotyping		
Primer: Mouse *Ch25h* Wild-type Reverse GTAGGCAGAAGCCCACGTAAGTGATG	Sigma-Aldrich	Recommended by Jackson Laboratories Primer #12262
Primer: Mouse *Ch25h* Mutant Reverse GCATCAGAGCAGCCGATTGTCTGTTG	Sigma-Aldrich	Recommended by Jackson Laboratories Primer #12263
Primer: Mouse *Ch25h* Common Forward CACAGTCTTAAGAAAAGTCGGCGGGG	Sigma-Aldrich	Recommended by Jackson Laboratories Primer #12261
Primer: Mouse *Ifnar1* Forward CTGGGAGCCAGGGCATAAC	Sigma-Aldrich	N/A
Primer: Mouse *Ifnar1* Reverse CCAGCCTTTCGGAGTGTGC	Sigma-Aldrich	N/A